LUND UNIVERSITY

Quantitative assessment of myocardial infarction: On the relationship between anatomy and electrophysiology using MRI and ECG

Engblom, Henrik

2006

Total number of authors:
1

Quantitative Assessment of Myocardial Infarction

On the Relationship between Anatomy and Electrophysiology using MRI and ECG

HENRIK ENGBLOM, MD

LUND UNIVERSITY

Doctoral Thesis
2006

Department of Clinical Physiology
Lund University, Sweden

Faculty opponent
Professor Robert B. Jennings M.D., Duke University Medical Center,
Durham, NC, USA

The public defense of this thesis for the degree Doctor of Philosophy in Medicine will, with due permission from the Faculty of Medicine at Lund University, take place in Föreläsningssal 1, Lund University Hospital, on Saturday, 30 September 2006, at 09.00.

Cover:
Delayed contrast-enhanced magnetic resonance (MR) images and a 12-lead electrocardiogram from a patient with a non-transmural infarction in the inferior left vetricular wall. In the three short-axis MR images and in the 2-chamber long-axis MR image, black myocardium is viable and white myocardium is infarcted (arrows). Pathological Q waves are seen in leads II, aVF, and V6 (arrows). For details see appended Paper I, Figure 5.

*Live and love
as if every day
was the last.
Sooner or later
you will be right....*
—G-I WIKSTRÖM

Contents

List of Publications

This thesis is based on the following papers, which in the text will be referred to by their Roman numerals.

My contribution to the studies was to take part in the design and data collection, and I was responsible for data analysis and writing of the manuscripts in all studies.

I. **Engblom H**, Hedström E, Heiberg E, Wagner GS, Pahlm O, Arheden H. Size and transmural extent of first-time reperfused myocardial infarction assessed by cardiac magnetic resonance can be estimated by 12-lead electrocardiogram. *Am Heart J.* 2005;150:920e1-9.

II. **Engblom H**, Carlsson MB, Hedström E, Heiberg E, Ugander M, Wagner GS, Arheden H. The endocardial extent of reperfused first-time myocardial infarction is more predictive of pathologic Q waves than is transmurality: A magnetic resonance imaging study. *Submitted*

III. **Engblom H**, Hedström E, Heiberg E, Wagner GS, Pahlm O, Arheden H. Time course and magnitude of infarct involution, functional recovery and electrocardiographic changes in patients with reperfused first myocardial infarction. *Submitted*

IV. **Engblom H**, Wagner GS, Setser RM, Selvester RH, Billgren T, Kasper J, Maynard C, Pahlm O, Arheden H, White RD. Quantitative clinical assessment of chronic anterior myocardial infarction with delayed enhancement magnetic resonance imaging and QRS scoring. *Am Heart J.* 2003;146(2):359-66.

Summary

Both presence and extent of myocardial infarction are important prognostic factors for mortality and quality of life in patients with ischemic heart disease. Thus, it is of great clinical importance to be able to diagnose and characterize myocardial infarction. One way to diagnose myocardial infarction is by using the 12-lead electrocardiogram (ECG). For estimation of infarct size and location from infarct-related ECG changes, the so called Selvester QRS scoring system can be used. This system is based on a forward modeling of the myocardial activation sequence. To further develop QRS scoring and for better understanding the pathophysiologic basis for infarct-related ECG changes, it is fundamental to understand how anatomic infarct characteristics relate to changes in the 12-lead ECG. The current reference standard for non-invasive visualization of myocardial infarction is delayed contrast-enhanced magnetic resonance imaging (DE-MRI). Hence, DE-MRI can be used to define the anatomic correlate to infarct-related QRS changes.

Paper I demonstrated that there was a good correlation between QRS score and infarct size by DE-MRI in patients with reperfused first-time infarction. Furthermore, the data showed that QRS score was related to infarct transmurality, whereas presence of Q waves was not indicative of transmural infarction.

Indeed, Paper II revealed that the endocardial extent of infarction was a stronger determinant for presence of pathological Q waves than was infarct transmurality in patients with reperfused first-time infarction.

In Paper III, the sequential changes of the infarction, left ventricular function and QRS score were studied in patients with reperfused first-time infarction. It was shown that almost two thirds of the total decrease in infarct size seen after one year occurred during the first week after infarction. Furthermore, regional wall thickening was shown to decrease progressively with increased infarct transmurality. Also, the timing and magnitude of decrease in infarct size assessed by DE-MRI was shown to correlate to the decrease in QRS score.

Finally, Paper IV demonstrated that in patients with chronic anterior infarction, frequently suffering from severe remodeling and left ventricular aneurysm, QRS score was only moderately correlated to infarct size assessed by DE-MRI.

In summary, DE-MRI has been used to describe the anatomical correlate to infarct-related QRS changes in acute, evolving, and healed myocardial infarction.

Populärvetenskaplig sammanfattning

Vid blodbrist till en del av hjärtmuskeln, t.ex. vid ett stopp i ett av hjärtats kranskärl, kommer delar av hjärtmuskeln att vara utsatt för risk att drabbas av infarkt. Hjärtinfarkt definieras som döda hjärtmuskelceller. Det är av stor vikt för en patient med kranskärlssjukdom att man kan skilja de delar av hjärtmuskeln som drabbats av infarkt ifrån de delar som inte drabbats av infarkt. Det har nämligen visats att såväl närvaro av infarkt som infarktens utbredning är av stor betydelse för patientens livskvalitet och livslängd. Därför är det av intresse att utveckla metoder som kan användas för att beskriva en hjärtinfarkts utbredning och lokalisation.

En av de mest använda hjärtundersökningar är elektrokardiografi (EKG), med vilken man undersöker hjärtats elektriska aktivitet. När hjärtat drabbats av en infarkt kommer hjärtats elektriska aktivitet att förändras. Dessa EKG-förändringar kan kvantifieras med hjälp av ett poängsättningssystem som kallas *Selvester QRS scoring*. För att bättre kunna utnyttja EKG för att beskriva en infarkts utbredning och lokalisation krävs en ökad förståelse för sambandet mellan infarktrelaterade EKG-förändringar och de delar av hjärtmuskeln som drabbats av infarkt.

Kontrastförstärkt magnetisk resonanstomografi (MR) kan användas för att i detalj avbilda vilka delar av hjärtmuskeln som drabbats av infarkt. I **delarbete I-IV** nedan användes därför MR som referensmetod för att bestämma hjärtinfarktens utbredning och lokalisation.

I **delarbete I** visades att *Selvester QRS scoring* kan användas för att uppskatta en infarkts storlek och dess tjocklek genom hjärtmuskelväggen (dess transmuralitet). Det visade sig också att tillkomst av en så kallad Q-våg i EKGet efter infarkt inte behöver betyda att infarkten sträcker sig genom hela muskeltjockleken som man tidigare antagit.

I **delarbete II** visades att uppkomst av Q-vågor istället beror mer på infarktens utbredning på vänsterkammarmuskelns insida än på dess transmuralitet.

I **delarbete III** undersöktes förändringar av infarktens utbredning, vänsterkammarens funktion och infarktrelaterade EKG-förändringar under ett år efter det att de studerade patienterna drabbats av hjärtinfarkt för första gången. Infarktstorleken mätt med MR minskade över tiden i samma utsträckning som

EKG-förändringarna normaliserades. Vänsterkammarens globala funktion återhämtade sig successivt under året medan dess regionala funktion återhämtade sig olika snabbt beroende på hur mycket infarkt som fanns i området.

I **delarbete IV** visades det att sambandet mellan *Selvester QRS scoring* och infarktstorlek mätt med MR var relativt svagt för patienter med äldre, utläkt infarkt i vänsterkammarens framvägg.

Sammanfattningsvis har MR använts för att beskriva hur en hjärtinfarkts utbredning påverkar hjärtats elektriska aktivitet både vid akut och äldre, utläkt infarkt.

Abbreviations

ATP	adenosine triphosphate
B	main magnetic field
^{11}C	carbon
CABG	coronary artery bypass grafting
CK-MB	creatine kinase isoenzyme MB
CT	computed tomography
cTnI	cardiac troponin I
cTnT	cardiac troponin T
DE	delayed contrast enhanced
DOTA	1,4,7,10-tetraazacyclododecane-1,4,7,10-tetraacetic acid
DTPA	diethylenetriaminepentaacetic acid
ECG	electrocardiography
EDV	left ventricular end-diastolic volume
EKG	elektrokardiografi
ESV	left ventricular end-systolic volume
^{18}F	fluorine
^{18}FDG	fluorodeoxyglucose
Gd	gadolinium
GRE	gradient-recalled echo
^{1}H	hydrogen
ICD	implantable cardioverter defibrillator
IHD	ischemic heart disease
IR	inversion recovery
LAD	left anterior descending artery
LCx	left circumflex artery
LV	left ventricle
LVM	left ventricular mass
M	net magnetization vector
MI	myocardial infarction

MR	magnetresonanstomografi
MRI	magnetic resonance imaging
mV	millivolt
^{13}N	nitrogen
NMR	nuclear magnetic resonance
^{15}O	oxygen
^{31}P	phosphorus
PCI	percutaneous coronary intervention
PET	positron emission tomography
^{82}Rb	rubidium
RCA	right coronary artery
RF	radio frequency
ROC	receiver operating characteristic
SPECT	single photon emission computed tomography
SSFP	steady state free precession
SV	stroke volume
T	tesla
^{99m}Tc	technetium
TI	inversion time
TIMI	thrombolysis in myocardial infarction
^{201}Tl	thallium
TTC	triphenyltetrazolium chloride
VF	ventricular fibrillation
VT	ventricular tachycardia

Chapter 1

Introduction

1.1 Ischemic heart disease

Ischemic heart disease (IHD) is the leading cause of morbidity and mortality in the western world.[1] Furthermore, it is the primary cause of heart failure.[2] The prevalence of IHD increases with increasing age[3] and in the year 2000 approximately 6.9 million Americans aged 65 years and older were estimated to suffer from IHD. The same year, 450000 deaths were attributable to the disease in this population. From a health economic perspective, this accounted for more than $50 billion in the year 2000. Since the elderly population is growing, we are facing an even bigger challenge handling patients with IHD in the future. To face this challenge, it is important to gain insight into the pathophysiologic basis of IHD and increase our ability to correctly diagnose and treat IHD.

Pathophysiology

Ischemic heart disease evolves from disease in the coronary arteries. Ischemia is defined as an insufficient oxygen supply of a tissue in relation to its oxygen demand. Hence, when the coronary arteries cannot deliver enough oxygen to supply the myocardial demands, myocardial ischemia occurs. The consequences of myocardial ischemia are dependent on several factors which will be discussed below in conjunction with the so called ischemic cascade.[4]

Before discussing the consequences of myocardial ischemia, it is important to understand the cause of it. The blood flow to the myocardium can be partially reduced due to coronary stenosis or completely absent due to coronary occlusion. The major pathophysiologic basis of coronary stenosis and occlusion is the formation of an atherosclerotic plaque in the coronary vessel wall. Coronary occlusion can also result from embolization[5] or spasm[6,7] of the coronary artery.

The evolution of an atherosclerotic plaque is initiated by accumulation of lipoproteins in the intima of the vessel wall. When these lipoproteins are subject to oxidative stress they can induce local cytokine release. The cytokines increase the expression of adhesion molecules enabling leucocytes to attach and migrate into the intima. As monocytes enter the intima their expression of scavenger receptors is increased, which results in an increased uptake of oxidative modified lipoproteins by the monocytes. This process promotes the monocytes to develop into so called foam cells. Local cytokine release also cause smooth muscle cells from the media of the vessel wall to migrate into the intima. By secreting extracellular matrix, smooth muscle cells contribute to the formation of the fibrous capsule surrounding the lipid-rich core of the evolving atherosclerotic plaque. The mechanical strength of this capsule is a major factor in regulating the propensity for a plaque to rupture. Thus, both impaired production and increased catabolism of extracellular matrix makes the plaque vulnerable to rupture.[8–10] As the plaque ruptures, the tissue factor within the plaque is exposed to the coagulation factors in the blood. Thus, plaque rupture promotes coronary thrombosis. In fact, plaque rupture accounts for approximately 75% of all fatal coronary thromboses.

The formation of a coronary thrombus and consequent reduction or absence of coronary blood flow is the initiator of the ischemic cascade (Figure 1.1). If the resulting ischemia is severe enough and persists for long enough the ultimate fate of the ischemic myocytes is irreversible injury (cell death). This irreversible injury is represented by myocardial infarction (MI) as the last step of the ischemic cascade. Before ischemia causes MI several alterations of the myocardium can be observed:

Diastolic dysfunction. Soon after the coronary artery has been occluded, diastolic dysfunction can be observed in the myocardium supplied by the occluded artery. The diastolic dysfunction is defined as impaired myocardial relaxation. The relaxation is the first to be affected by the ischemia since it is the most energy demanding process of the cardiac cycle. Normally, the myocytes relaxes by pumping cytosolic Ca^{2+} into the sarcoplasmatic reticulum or out of the cell. This process requires adenosine triphosphate (ATP). As the coronary artery becomes occluded, the oxygen supply to the myocardium distal to the occlusion is interrupted. The lack of oxygen results in a shift of the aerobic metabolism to anaerobic glycolysis within seconds.[11] The high-energy phosphate reserve, available predominantly as creatine phosphate, is almost completely exhausted after 30 seconds of ischemia. Thus, there is an imbalance between ATP production and consumption.[12] The latter exceeds the former, which initially results in dysfunctional myocyte relaxation.

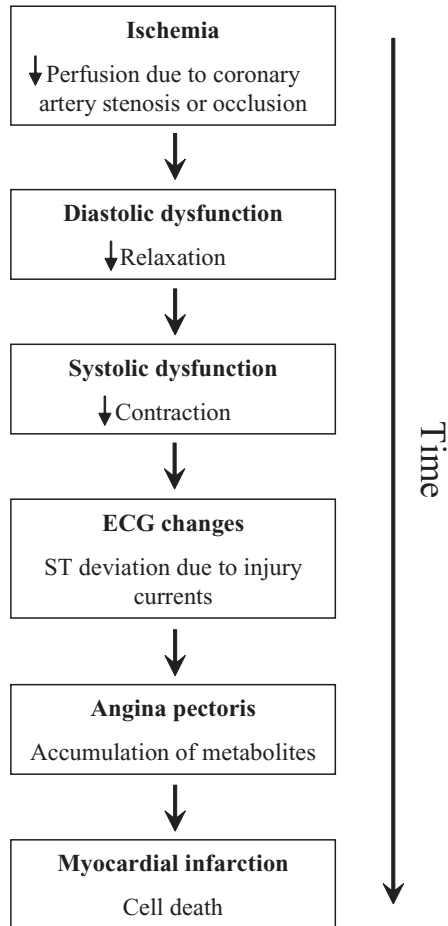**Systolic dysfunction.** As the ischemia persists, Ca^{2+} accumulates in the cytosol,

FIGURE 1.1 The ischemic cascade. The sequential events occurring after onset of ischemia are illustrated.

the cytosol becomes acidotic and exhibits a rise in phosphate concentration.[13, 14] This eventually causes impairment of myocyte contractility and systolic dysfunction which is the next step in the ischemic cascade.

ECG changes. The earliest and most consistent electrocardiographic alteration due to acute ischemia is ST-segment deviation resulting from injury currents induced in the border zone between ischemic and non-ischemic myocardium.[15–17] These ST-segment changes arise from reduction of the resting membrane potential, decrease of action potential duration and decrease in rate of rise and amplitude of the initial, rapid depolarization phase of the action potential.[18]

Angina pectoris. Eventually the accumulation of metabolites in the ischemic myocardium will cause development of chest pain, so called angina pectoris.[19] The chest pain is often experienced in conjunction with radiating pain in the arms, the neck, the jaw, the shoulders, or the back. The accumulated metabolites (including adenosine) stimulate afferent cardiac nerves that fuse with afferent nerves from the organs mention above, explaining the radiation of pain.

Myocardial infarction. If the ischemia is severe enough and persists long enough without restoration of blood flow, the ultimate fate of the myocytes supplied by the occluded artery is irreversible injury (cell death). As the ischemia persists even further, the MI will evolve from the endocardial border progressing toward the epicardium in a wave-front manner.[20] If there is no restoration of blood flow the MI will ultimately involve the full thickness of the myocardial muscle wall. This is called transmural MI. Thus, the duration of ischemia is a major determinant of the extent of MI.

Ischemic preconditioning and collateral flow

In addition to the duration of ischemia, there are other factors that affect the consequences of coronary occlusion. If the myocardium is subject to a few repetitive short ischemic episodes, it has increased its protection against subsequent prolonged ischemic episodes. This phenomenon, first described by Murry *et al*,[21] is called ischemic preconditioning. Ischemic preconditioning has been shown to reduce the level of ST-segment deviation[22] and decrease MI size.[23, 24] The mechanisms for the preconditioning are complicated and not fully understood. They involve a much lower utilization of ATP, delayed development of acidosis, and slower accumulation of lactate in preconditioned compared to the non-preconditioned myocardium. This suggests that preconditioned myocardium has a reduced energy demand, and consequently, a delayed myocyte death when the blood flow is interrupted.[25, 26] The concept of ischemic preconditioning in hu-

mans has been supported by clinical studies.[27, 28]

Another factor that determines the extent of MI after coronary occlusion is the degree of collaterals, defined as vascular channels that interconnect coronary arteries. If present, it is the collaterals that supply the ischemic myocardium in the situation of total or sub-total occlusion.[29] The collaterals are preexisting, immature and nonfunctional vessels and their density vary between species.[30] The collaterals can develop into functional vessels by external stimuli such as inflammation, shear stress, exercise, and hypoxia.[31] The latter is probably the most important in coronary artery disease. It has been shown that the severity of a coronary stenosis must exceed 70% in humans for collaterals to develop. For coronaries with >70% stenosis the amount of collateral flow is closely related to the degree of stenosis.[32] This can explain why patients with severe angina pectoris often have well developed collaterals. These patients have one or more tight stenoses that cause episodes of myocardial ischemia and hypoxia which stimulate the collateral development to the ischemic myocardium. If the affected vessel subsequently occludes, the myocardium distal to the occlusion is supplied by collateral flow from other coronary arteries. Indeed, it has been shown that if the collateral flow exceeds 28% of the normal maximal blood flow in the occluded artery, no ischemia is seen after occluding the artery by balloon angioplasty.[33] Thus, in acute MI, collateral flow can decrease MI size, improve left ventricular (LV) function, and improve survival.[34, 35]

Diagnosing myocardial infarction

Myocardial infarction can be defined from several perspectives related to clinical, pathologic, electrocardiographic, imaging and biochemical characteristics.[36] The classic clinical diagnosis of MI, according to the World Health Organization (WHO), is defined by a combination of two of the three following manifestations: 1) typical symptoms such as chest pain, radiation pain, shortness of breath, weakness, nausea, or loss of consciousness 2) acute ECG changes including ST-segment deviation, hyperacute T-wave elevation, or Q-wave development 3) biochemical markers of infarcted myocardium present in plasma such as creatine kinase isoenzyme MB (CK-MB) and cardiac troponin T or I (cTnT or cTnI).

Pathology. The definition of MI is, as discussed above, cell death due to prolonged myocardial ischemia. The cell death can be identified by specific histological patterns such as coagulation or contraction band necrosis. By pathology, the MI can be localized and quantified as well as classified according to the timing of the MI (acute, healing, or healed) by description of the ultrastructure of the MI and the presence of polymorphonuclear leucocytes.

ECG. The ECG can show signs of acute transmural ischemia such as significant ST-segment deviation[37, 38] or tall T waves,[39, 40] but also signs of non-acute MI such as alterations of the QRS complex[41–43] or T-wave abnormalities[44] can be observed. During the MI healing process infarct-related ECG changes may resolve.[45–49] Electrocardiographic signs of ischemia and MI will be discussed further in subsequent chapters.

Imaging. Different imaging techniques utilize different aspects associated with MI. Impaired global and regional LV function due to ischemia or infarction can be assessed with imaging techniques such as echocardiography, gated single photon emission computed tomography (SPECT), gated positron emission tomography (PET), gated computed tomography (CT), and cardiac magnetic resonance imaging (MRI). Cardiac MRI is considered the reference method for assessment of cardiac function. Echocardiography, gated SPECT, and cardiac MRI are also frequently used to assess myocardial function at stress to reveal myocardial dysfunction due to stress-induced ischemia. These techniques can also be used to assess myocardial perfusion at rest and at stress. For quantitative assessment of myocardial perfusion, PET is considered the reference method. To evaluate the coronary arteries with regard to presence of stenosis or occlusion, invasive coronary angiography by x-ray fluoroscopy is the reference method. In contrast to invasive coronary angiography, CT and MR angiography can be used to noninvasively depict the coronary arteries. For noninvasive infarct visualization, delayed-contrast enhanced MRI (DE-MRI) is considered to be the reference method. Delayed-contrast enhanced CT has also shown promising results with regard to noninvasive infarct visualization. The different cardiac imaging modalities will be discussed further below.

Biochemical markers. The most common biochemical markers used to diagnose acute myocyte death are CK-MB, cTnT, and cTnI. The CK-MB is a cytosolic protein which leaks out of the myocyte as its cell membrane ruptures. The troponins also leak out of the cytosol as the myocytes die. In addition to a cytosolic pool, the troponins also exit bound to the tropomyosin complex. Thus, the troponins remain elevated for a longer time after acute MI than does CK-MB. By serial sampling of the two markers the peak concentration can be determined, which has been shown to correlate well with MI size.[50–52]

Different outcomes after acute infarction

If the duration of ischemia is prolonged enough to cause MI, there are several factors determining the subsequent cardiac function and patient outcome. As discussed above, in the absence of collateral flow, the MI transmurality increases

progressively with increased duration of ischemia.[20] The MI transmurality has been shown to be an important determinant for functional recovery after acute MI[53] or after revascularization in chronic ischemic heart disease.[54] In addition to duration of ischemia, the localization of the occlusion is also important for the resulting MI size. The more proximal the site of occlusion the more myocardium is at risk. Furthermore, the different coronary arteries supply different amounts of myocardium.[55] Usually, the left anterior descending artery (LAD) is the dominating vessel with regard to the amount of myocardium supplied by it. Thus, a proximal LAD occlusion usually results in a larger MI than an occlusion in the proximal right coronary artery (RCA), given the same duration of ischemia and equal amounts of preconditioning and collateral flow. The larger the MI the lower the cardiac function.[56]

Complete recovery. If the infarct is aborted or is very small, either because of short duration of ischemia or significant collateral flow, there may be complete normalization of cardiac function after the acute coronary occlusion.

Myocardial stunning. The normalization of function can be preceded by a period of transient decrease in cardiac function (hypokinesia) caused by myocardial stunning. Stunned myocardium has been defined by Braunwald and Kloner as "prolonged, postischemic dysfunction of viable tissue salvaged by reperfusion."[57] Thus, myocardial stunning may occur even without MI. The timing and degree of recovery of cardiac function in stunned myocardium depends on the duration and severity of ischemia and on the adequacy of the restoration of blood flow.[58]

Myocardial hibernation. A reduction in myocardial function can also be caused by a persistent decrease in blood flow due to a tight coronary stenosis. The blood supply to the myocardium distal to the stenosis is too low for the myocardium to contract properly, but enough for the myocardium to remain viable. This phenomenon is called myocardial hibernation and has been described as "a state of persistently impaired myocardial and LV function at rest due to reduced coronary blood flow that can be partially or completely restored to normal if the myocardial oxygen supply/demand relationship is favorably altered, either by improving blood flow and/or by reducing demand."[59] Thus hibernating myocardium has the potential to recover function in contrast to infarcted myocardium.[60–62]

Myocardial remodeling. In the situation where the MI is large enough to cause permanent, partial loss of cardiac function there is a need to compensate for this functional loss. The changed loading conditions stimulate myocardial remodeling, which can alter the topography of both infarcted and viable myocardium. An early alteration of the infarcted myocardium, especially the transmural MI, is

infarct expansion. Infarct expansion is defined as "acute dilatation and thinning of the area of infarction not explained by additional myocardial necrosis."[63] Depending on the amount of MI, the remodeling process spans from well adapted compensatory hypertrophy (positive remodeling) to pronounced wall thinning and aneurysm formation (negative remodeling). As the MI size increases, the risk of ventricular dilatation and heart failure increases.[56]

Heart failure. Heart failure is defined as "the pathophysiologic state in which the heart is unable to pump blood at a rate commensurate with the requirements of the metabolizing tissue or can do so only from an elevated filling pressure.".[64] The development of heart failure after acute MI is a poor prognostic sign.[65–67] In fact, heart failure has been shown to have a 1-year mortality of 38% and a 5-year mortality of >70%,[68] which is worse than for most forms of cancer. Risk factors for developing heart failure at admission and early after acute MI includes high age,[65,66,69] female sex,[65,66,69,70] diabetes,[65,66,69,71] hypertension,[65,66,69,71] and other comorbidities including preexisting coronary artery disease,[66,69] stroke,[65,69] and renal dysfunction.[66,72]

Malignant arrhythmias. Another possible outcome after acute coronary occlusion is development of ventricular tachycardia (VT) or ventricular fibrillation (VF). Ventricular fibrillation can occur before the development of MI and is a common cause of sudden death in conjunction with acute coronary occlusion.[73] Approximately 60% of the VF episodes occur within 4 hours and 80% within 12 hours of the onset of symptoms.[74]

Ventricular tachycardia and VF may also occur as the MI is established and healed. The risk of developing VT and VF increases with increasing MI size.[75,76] Re-entry circuits may develop within the infarcted myocardium which then can function as a substrate for inducing of ventricular arrhythmias.

Dyssynchrony. When a large portion of the LV is infarcted, often caused by a LAD occlusion, there is a risk for development of a LV aneurysm.[77] The aneurysm is characterized by akinetic or dyskinetic wall motion. This results in a non-uniform pattern of ventricular contraction and relaxation, which is called mechanical dyssynchrony. The mechanical dyssynchrony reduces the efficiency of ventricular filling and ejection and contributes both to diastolic and systolic dysfunction.[78,79] Non-transmural MI can also cause dyssynchrony by electrophysiological alterations. The viable epicardial rim superficial to the MI is no longer activated from the underlying endocardium. The depolarization has to propagate around the MI to reach the spared epicardial myocardium. Since the depolarization is delayed, the contraction of the myocardium in this region is also delayed compared to the contraction of remote, non-infarcted myocardium.

Thus, dyssynchrony can originate from non-uniform depolarization of the myocardium after MI.

Therapy

The main goal of the therapy in acute coronary occlusion is to restore the blood flow to the ischemic myocardium in order to minimize the extent of MI. The restoration of blood flow can be achieved either by pharmacological or mechanical intervention.

The aim of the pharmacologic intervention in the acute phase is to promote the fibrinolytic system to dissolve the occluding thrombus (thrombolysis) and to prevent further thrombotization (anticoagulation and platelet inhibition). Thrombolysis has several drawbacks: First, it is not possible to directly assess if the epicardial blood flow is restored. Second, blood flow is achieved by this therapy only in about three fourths of the infarct-related arteries.[80] Furthermore, epicardial blood flow is completely restored in the infarct-related artery (Thrombolysis In Myocardial Infarction [TIMI] grade 3)[81] only in about half of the patients receiving thrombolysis.[80]

Mechanical restoration of blood flow to the ischemic myocardium can be achieved either by percutaneous coronary intervention (PCI) or coronary artery bypass grafting (CABG). By PCI, practically all infarct-related arteries can be opened, with resulting TIMI 3 flow in approximately 90% of the patients.[82] Furthermore, the use of stents, anticouagulants and platelet inhibitors in conjunction with the PCI can increase the proportion of persistently opened arteries and decrease the risk of complications to the acute MI.[83] Thus, PCI is superior to thrombolysis with regard to restoring the arterial blood flow in the setting of acute MI. In a meta-analysis of 23 prospective, randomized clinical trials, Keeley *et al*[84] showed that PCI resulted in lower mortality, fewer reinfarctions and strokes both in the short- and long-term perspective compared to thrombolysis. The use of CABG in the situation of ongoing acute MI is limited to the patients with angiographic evidence of complicated coronary disease, not suitable for PCI.

To prevent negative remodeling in the post MI period, several drugs are available: angiotensin converting enzyme inhibitors,[85] angiotensin receptor blockers,[86] and ß-blockers.[87]

Acetylsalicylic acid[88, 89]and platelet aggregation inhibitors[90, 91] are used to prevent the affected vessel from re-occluding with consequent improved patient prognosis. Glycoprotein receptor IIb/IIIa inhibitors can be used to reduce thrombotic complications associated with PCI.[92]

The need for mechanical therapy in the post MI period depends on the complications. If the MI results in aneurysmal deformation of the LV, aneurysmectomy can improve LV function by decreasing the mechanical dyssynchrony.[93]

Electrophysiological dyssynchrony can be treated by epicardial pacing of the viable rim of myocardium superficial to the MI. By transvenous application of an epicardial pacing catheter, the depolarization of the viable rim can be optimized by synchronization with the depolarization of the rest of the myocardium.

To prevent sudden death in patients with documented prolonged VT and/or VF in the post-infarction period, implantation of an implantable cardioverter defibrillator (ICD) can be performed.[94–96]

1.2   Cardiac imaging

There are several imaging modalities capable of depicting the heart in vivo. Different modalities utilize different properties of physics in order to depict different characteristics of the cardiac anatomy and physiology to provide diagnostic information regarding the heart. There are different advantages and drawbacks with different images modalities that need to be considered when choosing imaging modality. The following section on cardiac imaging gives a brief overview of the most widely used cardiac imaging techniques, with specific focus on cardiac magnetic resonance imaging (MRI).

X-ray

Plain X-ray. X-rays have been used in medical imaging for over a century now. By transmitting X-rays through a part of the body and detecting them on the other side, contrast between different tissues is obtained. Different tissues have different density and will absorb or scatter (attenuate) the X-rays differently. High-density tissue such as bone will attenuate more than low-density tissue such as the lungs. Thus, the contours of the heart can be traced from a plain x-ray image. Plain X-ray, however, provides little information about cardiac anatomy and function.

X-ray fluoroscopy. X-ray fluoroscopy is the use of X-rays to image the body in real time. This technique can be used to evaluate ventricular function (ventriculography),[97] but the most common application for x-ray fluoroscopy in cardiac imaging today is coronary angiography. With this technique the coronary arteries can be visualized after injection of an iodine-based, attenuating contrast agent. This way coronary stenoses and occlusions can be detected from silhouettes of the coronary lumen. X-ray fluoroscopy has an excellent spatial resolution of about 0.25×0.25 mm and a high temporal resolution of about 6 ms. The major advantage with coronary angiography is that it enables intervention in the same session if needed. This is, however, an invasive imaging technique associated with 0.1% mortality.[98]

Computed tomography. Another technique where X-rays are used to acquire image contrast is computed tomography (CT). By sliding the patient through a bore surrounded by a rotating X-ray transmitter and a detector, multiple tomographic images can be acquired. With a 64-channel CT-scanner a complete ECG-gated cardiac exam can be performed in a few minutes providing an image resolution of $0.6 \times 0.6 \times 0.6$ mm.[99] The excellent spatial resolution in combination with administration of an attenuating intravenous contrast agent makes this a promising technique for non-invasive coronary imaging.[99, 100] Since calcium attenuates X-rays, cardiac CT can be used to detect calcification in the coronary arteries. The burden of calcified plaques can be quantified by so called calcium scoring. Calcium scoring has been shown to have prognostic value in patients at risk for coronary artery disease.[101] By ECG-gating global LV function can be assessed.[102–104] However, the temporal resolution is still somewhat low (170–200 ms). Recent studies have shown that contrast enhanced CT may be used to identify areas of MI.[105]

Since X-rays are a form of ionizing electromagnetic radiation with the potential to damage human DNA, imaging modalities utilizing this radiation are associated with risk of initiating malignant processes.[106] Thus, X-ray modalities are not well suited for serial follow-up studies especially not in younger populations.

Echocardiography

In echocardiography, images of the heart are generated by transmission, reflection and detection of ultrasound emitted and detected by a transducer placed on the chest wall. Echoes are generated when sound travel between tissues with different acoustic impedances. The acoustic impedance is the product of the velocity of sound in the tissue and the density of the tissue. Thus, the myocardium and other cardiac structures such as valve leaflets can be visualized by this technique. Echocardiography can be performed in both in one, two, and three spatial dimensions. The three dimensional technique has shown great ability to accurately determine LV volumes and function.[107] Echocardiographic images have a spatial resolution of about $1 \times 2 \times 2$ mm and temporal resolution of approximately 20 ms, depending on the technique used.

In addition to depicting the cardiac anatomy, echocardiography can be used to measure velocities. This can be achieved by utilization of the Doppler principle, stating that the frequency of reflected sound waves changes according to the velocity and direction of the moving object that they are reflected against. The Doppler technique is frequently used to visualize blood flowing through the heart, enabling detection of cardiac malformations, e.g. of valves, myocardial walls, or great vessels.

The assessment of velocities of different parts of the myocardium can be used

to assess regional myocardial function.[108] Global and regional LV function can be assessed both at rest and during stress.

Echocardiography is a technique free of ionizing radiation and is widely available. Portable echocardiography machines can easily be managed in the emergency room, which makes this technique feasible for diagnosing impaired function in the setting of acute MI. A major drawback with this technique, however, is that diagnostic images can be difficult to acquire in up to 25% of the patients due to body habitus that limits the acoustic window. Furthermore, the image quality and diagnostic accuracy is operator dependent.

Single photon emission computed tomography

Myocardial perfusion can be visualized by the use of single photon emission computed tomography (SPECT). This is a nuclear medicine imaging modality which uses an intravenously administered radioactive tracer to depict myocardial perfusion. The biological properties of the radioactive tracer determine which physiological processes will be visualized. The three most common tracers are ^{201}thallium thallous chloride (^{201}Tl), ^{99m}technetium 2-methoxy-isobutyl-isonitrile (^{99m}Tc-sestamibi) and technetium 1,2-bis[bis(2-ethoxyethyl) phosphino] ethane (^{99m}Tc-tetrofosmin). The ^{99m}Tc tracers are readily extracted from the blood within minutes and remain in myocytes containing viable mitochondria. Thus, myocardial perfusion SPECT can by performed up to three hours after injection of the tracer. The ^{201}Tl tracer is also readily extracted by viable myocytes. However, this tracer stays in the blood stream and can redistribute into the myocardium. This property can be utilized for viability assessment.[109]

After injecting the radioactive tracer the patient is placed in a gamma camera. The gamma camera contains detectors for emitted photons (gamma radiation) from decaying radioactive tracers in the perfused, viable myocardium.[110] Regions with reduced or absent perfusion can be identified both at rest and during stress. The SPECT images have an approximate spatial resolution of $10\times10\times10$ mm and a temporal resolution of approximately 70 ms. Similarly to CT, this image acquisition can be ECG gated, enabling assessment of LV function.[111–113]

Positron emission tomography

Positron emission tomography is, like SPECT, a nuclear medicine imaging technique involving detection of a radioactive tracer administered into the blood stream. The detectors surround the patient and detect photons emitted from collisions between positrons and electrons. The positron is emitted as the radioactive tracer decays. When the positron hits an electron a so called annhilation process occurs in which two photons are emitted in opposite directions. By detecting

these photons at the same time in opposite detectors in the detector ring (coincident detection) it is possible to derive the location of the emitting source along a straight line between the detectors. Images can be reconstructed by deriving information about coincident detection along multiple lines between detectors.

The radioactive tracers used in PET (^{11}C, ^{13}N, ^{15}O, ^{18}F, and ^{82}Rb) can be incorporated into a biologically active compound, i.e. the glucose analogue ^{18}F-fluorodeoxyglucose (^{18}FDG). ^{18}FDG can then be used to assess myocardial metabolism. Myocardial blood flow can be quantified in ml/g/min using i.e. ^{13}N-ammonia.

As earlier mentioned, PET is considered the reference method for quantifying myocardial perfusion.[114] However, it can also be used to assess myocardial function by ECG-gated image acquisition.[115, 116] In addition, PET with ^{18}FDG can be used to assess myocardial viability.[117]

The image acquisition is undertaken during free breathing which is a limitation. The effective spatial resolution achieved with PET is typically $5 \times 5 \times 5$ mm. The temporal resolution is in the same order of magnitude as for SPECT, approximately 70 ms.

Cardiac magnetic resonance imaging

Magnetic resonance imaging (MRI) is an imaging modality based on quantum mechanics. It can be used to obtain images of the human body in any given imaging plane. Images can be acquired in different ways enabling depiction of different physiological and pathophysiological processes. This imaging technique is free of ionizing radiation which makes it suitable for repeated examinations when necessary.

Background

The MRI technique has generated four Nobel Prizes.

In 1952, Felix Bloch and Edward Purcell, were awarded the prize in physics for independently discovering the phenomenon of magnetic resonance in 1946.

In 1991, Richard Ernst was awarded the prize in chemistry for his work on pulsed Fourier Transform in nuclear magnetic resonance (NMR) and MRI. The Fourier transform is necessary for decoding the acquired MR signals into diagnostic images.

In 2002, Kurt Wüthrich was awarded the prize in chemistry for his development of NMR spectroscopy for determining three dimensional structures of biological macromolecules in solution.

Finally, in 2003, Paul C. Lauterbur and Sir Peter Mansfield shared the prize in medicine or physiology for their discoveries concerning the use of gradients in

MRI which have made the method feasible for clinical imaging.

In 2003, approximately 10,000 MRI units were in use world wide and approximately 75 million MRI scans were performed. The MRI technique is still young and continues to grow, particularly in the field of cardiac imaging.

Basic principles

The basic quantum physics behind MRI relies on particle spins. Spin is a fundamental property of nature and applies to protons, electrons and neutrons. Spins can be positive or negative depending on the state of energy. The direction of a spin can be manipulated by the supply of energy. Nuclei with unpaired protons such as ^{1}H, ^{31}P and ^{19}F are of interest for MRI since spins can pair up and cancel out when protons come in pairs.

To understand how particles with spin behave in a magnetic field it is easiest to consider ^{1}H as an example. In fact, ^{1}H consists of a single proton and is the nuclei used to acquire the signal in almost all clinical MRI. The proton spins (precess) around its own axis and can be thought of as a small electrical current that gives rise to a small magnetic moment vector. Thus, the proton behaves like a tiny magnet with a north and a south pole. When this tiny magnet is placed in an external magnetic field, the spin vector of the proton aligns with the external magnetic field. If the external magnetic field is defined as B, the spinning proton can absorb a photon of frequency ω (the Larmor frequency). The Larmor frequency ω depends on the gyromagnetic ratio, γ of ^{1}H.

$$\omega = \gamma B$$

The gyromagnetic ratio, γ for ^{1}H is 42.58 MHz / Tesla (T). The ability to absorb energy only from photons with a specific frequency of resonance is the source of the word *resonance* in magnetic resonance imaging.

When the proton is placed in the external magnetic field B, its spin vector can align with or against B. The alignment with B has a somewhat lower energy state than alignment against B. Thus, the probability for a proton spin vector to align with B is somewhat higher than for alignment against B.

These are the basic principles governing the use of protons to acquire images of the human body.

The magnet

The magnet consists of 1) a main magnet, responsible for the main magnetic field 2) radio frequency coils, used to transmit and receive radiofrequency pulses, and

3) a gradient system, used to spatially locate the MR signal.

The main magnet. The main magnet consists of a metal wire, most often wrapped around a circular gantry. The metal wire is cooled by liquid Helium resulting in supraconduction. Thus, the resistance is approximately zero and the electrical current that is supplied to the magnet as it is started remains in the magnet. The electrical current through the metal wire generates a strong magnetic field. The typical field strength used for cardiac imaging is 1.5 T. By comparison, the earth's magnetic field strength is 0.00005 T. As the patient is placed in supine position in the magnet, the main magnetic field forces the ^{1}H protons within the body to align according to B. As discussed above there will be a slightly greater number of spin vectors aligning with B compared to spin vectors aligning against B. Thus, there is a net magnetization vector (M) in the positive direction of B. The small M generated by the protons cannot be detected when it is in the same direction as B. Thus, there is a need for manipulation of M to change its direction and make it detectable. Here is where the radio frequency coils come into play.

Radio frequency coils. There are two different types of radio frequency (RF) coils: a transmitting coil and a receiving coil. The RF-transmitter coil transmit energy in RF pulses with a desired frequency into the patient within the scanner, whereas the RF-receiver coil detects the signal that is emitted back from the patients. As recalled from above, when the frequency of the transmitted RF pulse reassembles the Larmor frequency, this energy can be absorbed by the spinning protons within the body. This energy absorption causes M to change direction, deviating from B at a given angle. As the protons continue to precess they give rise to a varying magnetic field with a component perpendicular to B. This varying magnetic field generates signal currents (echoes) which can be detected by the RF-receiver coil. This echo is proportional to the number of ^{1}H protons that were excited by the RF-pulse. The amount of ^{1}H protons and the ability for the ^{1}H protons to interact with their surroundings are different for different tissues. These properties give rise to the contrast between different tissues in MRI. In summary, it is possible to make M deviate from B and to detect signal from the excited tissue by the use of RF coils. The next step is to enable excitation only of the tissue of interest and not the entire patient, and to localize of the spatial origin of the signal. To accomplish this, a way to spatially encode the origin of the signal detected by the RF-receiver coil is needed. This is the function of the gradient system.

The gradient system. The gradient system consists of gradient coils with potential to affect the main magnetic field. By doing so, the gradient coils introduce a linear magnetic field gradient which is a variation of the magnetic field with

regard to position. As discussed above, the Larmor frequency, ω is directly proportional to the magnetic field strength. Thus, by applying a linear magnetic field gradient it is possible to excite only the specific slices of the body in which the ω is in resonance with the RF-pulse. The linear magnetic field gradient can be applied in any given direction. Hence, the image plane can be positioned and angled arbitrarily in all three spatial dimensions. Once the desired image slice is excited, the signal from the different tissues within the slice must be discriminated. This is also accomplished by the gradient system. Encoding of signal in the x and y direction within the slice is accomplished by applying a gradient in the y direction prior to signal detection and by applying a gradient in the x direction during signal sampling. The y direction gradient causes a phase shift which remains during the sampling of the signal. This is called phase encoding of the signal. The gradient in the x direction causes a shift in spin frequency along the x direction. This is called frequency encoding of the signal. In summary, by applying a linear magnetic field gradient, a specific image slice can be chosen, in which signal from different tissues can be localized by phase and frequency encoding. In order for the encoded signal to be transformed into interpretable anatomical images it has to be further manipulated. Thus, it is necessary to enter the k-space.

K-space. The raw signal detected by the RF receiver coil is acquired in the so called spatial frequency domain, or k-space. Signal is usually sampled in lines of raw data (lines in k-space). The number of lines and the position of the lines in k-space determine the spatial or, if dynamic imaging is employed, also the temporal resolution of the final image(s). The information that could be retrieved by studying the raw data in k-space without any post processing, is minimal. In k-space, the signal is still encoded according to phase and frequency and not according anatomical landmarks. Once the k-space contains enough information, enough lines, to derive the desired anatomical information, a mathematical operation called Fourier transformation is applied. The Fourier transform uses the encoded signal to derive excellent anatomical images, very well suited for diagnostic purposes. The spatial resolution is typically $1.2 \times 1.2 \times 8$ mm and temporal resolution for dynamic images approximately 30 ms.

T1 and T2 relaxation

As mentioned earlier, the signal that is detected by the RF-receiver coil is dependent on the number of ^{1}H protons and the tissue surrounding them. This difference in signal is used to achieve contrast between different tissues in the image. There are two variables used to describe the magnetic properties of a given tissue: T1 and T2 relaxation.

When the protons in a given image plane have been excited by an RF pulse,

the net magnetization vector (M) starts to realign to the main magnetic field (B). This is called relaxation. The time it takes for M to realign with B is dependent on the angle by which the M was flipped from B (the flip angle) and on the ability for the excited protons to emit energy to its surrounding. The rate with which M regains its component in the direction of B is called T1 relaxation. The rate with which the component perpendicular to B is lost is called T2 relaxation. T1 is defined as the time when M has regained 63% of its original component in the direction of B. T2 is defined as the time when 37% of the M component perpendicular to B remains. T1 in human tissue typically varies between 300 and 1500 ms, whereas T2 varies between 50 and 500 ms. Knowledge about the T1 and T2 relaxation properties for different tissues has enabled the design of specific pulse sequences in which the timing and duration of RF pulses is optimized for visualization of a specific tissue or a specific pathophysiological process.

Cardiac function

In addition to static anatomical imaging of different tissue characteristics, it is possible to perform dynamic MR imaging, so called cine imaging. There are several challenges in performing dynamic cardiac imaging. First, the heart is moving inside the chest during the respiratory cycle. Second, the heart has an intrinsic movement during the cardiac cycle.

The respiratory motion can be compensated by imaging during breath holding. Most cardiac sequences on today's MR scanners can be acquired within a single breath hold. For three dimensional coverage of the heart repeated breath holds may be required, although development of new, faster image acquisition techniques might solve this problem in the future.[118] Still, some patients have difficulties in holding their breath long enough for adequate image acquisition.

To compensate for the intrinsic cardiac movement during the cardiac cycle, imaging can be triggered by ECG. The most common triggering strategy is retrospective ECG gating. With retrospective gating, MR signals are sampled during the entire duration of the image acquisition (typically 5 s for depiction the cardiac cycle with a temporal resolution of 30-40 ms in one image plane) in conjunction with a simultaneous registration of the ECG. After the image acquisition, the sampled signal is matched to the time point in the cardiac cycle in relation to the R wave. This way a full coverage of the cardiac cycle can be obtained. ECG triggering can sometimes be problematic due to disturbances of the ECG caused by the magnetic field. Also, if the patient has arrhythmia, such as atrial fibrillation, the ECG gating can be difficult. To overcome these problems, self-gating approaches have been proposed.[119, 120]

Cardiac function is usually determined from short-axis images of the heart. The short-axis image plane is determined in a standardized fashion[121] to ensure

accurate functional assessments in follow-up examinations. Currently, in clinical routine as well as for research purposes, a so called steady state free precession (SSFP) sequence is usually used for functional assessments. The SSFP sequence provides images with great contrast between the cardiac blood pool and the myocardium without the use of any contrast agents. This contrast is achieved by utilizing the ratio between T2 and T1.

Regional function can be assessed by the use of a so called grid-tagging sequence. With grid tagging, the signal in the tissue along a grid pattern is cancelled in end-diastole. The grids are then deformed as the muscle moves during systole. Thus, the grid-pattern will be less deformed or not deformed at all in regions of dysfunctional myocardium.

Myocardial perfusion can be assessed by so called first-pass perfusion assessment. The in-flow of the contrast agent can be depicted by acquiring images at the same time as a gadolinium (Gd)-based contrast agent is being injected intravenously. The in-flow of contrast agent is seen as hyperenhancement of the perfused myocardium, typically acquired in 3-5 short axis slices simultaneously. Regions with decreased or absence of perfusion appear hypoenhanced.

Flow can also be assessed by cardiac MRI with high accuracy and precision. Flow quantification by MRI is based on velocity encoding. By using velocity sensitive pulse sequences, it is possible to acquire images in which the gray scale in each volume element (voxel) is directly proportional to the velocity of the voxel. The velocity encoding can be performed both in-plane and through-plane. When applying through-plane velocity encoding in imaging planes perpendicular to the great vessels, the blood flow through them can be determined with very high accuracy.[122] Velocity encoding can also be applied to assessment of myocardial muscle velocity.[123] This technique enables detailed assessment of regional myocardial strain.

Infarct assessment

During the last few years, MRI has evolved as the reference method for in-vivo visualization of MI. As discussed previously, both presence and extent of MI in patients with IHD are important with regard to choice of therapy and patient prognosis. For patients with IHD, the presence of MI is a bad prognostic sign.[124] Thus, there is a growing interest and progressive increase in clinical referrals for MRI viability assessments.

The two most important aspects of MI visualization with MRI are 1) the use of a paramagnetic contrast agent and 2) an appropriate pulse sequence to visualize the effects of the contrast agent.

Paramagnetic contrast agents. The paramagnetic contrast agents used in car-

diac MRI are Gd-based. Gadolinium has paramagnetic properties that affect its surroundings by shortening of the T1 relaxation.[125] Thus, it is not the gadolinium itself that is visible in the MR image, bur rather its paramagnetic effect on its surroundings. Gadolinium ions in their free form are toxic and need to be chelated to a ligand in order to reduce toxicity.[126] Such ligands include 1,4,7,10-tetraazacyclododecane-1,4,7,10-tetraacetic acid (DOTA) and diethylenetriamine-pentaacetic acid (DTPA), which are explicit extracellular agents. After intravenous injection of the Gd-based contrast agent, it distributes into the extracellular space of perfused tissue and reaches a steady state after approximately 20 min.[127]

Delayed contrast-enhanced MRI. The T1 relaxation will be shorter in tissue containing more Gd compared to tissue with less Gd. In order to utilize the fact that different tissues have different T1-relaxation rates, an inversion recover (IR) sequence can be applied. In short, this sequence consists of an inversion pulse (flipping M 180°) followed by an inversion time (TI). The TI is the delay between excitation by the RF transmitter coil and the sampling of the signal by the RF receiver coil. The TI can be adjusted to null the signal from a tissue with a given T1. For example, as the Gd-based contrast agent has distributed and reached steady state, TI can be adjusted to null the signal from viable myocardium (Figure 1.2). This way, myocardium that contains more Gd than viable myocardium will hyperenhance and the viable myocardium will appear black. This is the source for the term delayed-contrast enhanced MRI (DE-MRI) used to visualize MI.

Distribution volume. As the Gd-based contrast agent is injected it will distribute freely into the extracellular space. Thus, the amount of contrast agent is directly proportional to the relative amount of extracellular space, the distribution volume of the contrast agent.[128–131] This is the fundamental pathophysiological basis for visualization of MI by MRI. In the situation of acute MI, the cell membrane of myocytes in the infarcted area has ruptured. When the myocytes have lost their cellular integrity the former intracellular space now becomes one with the extracellular space. Thus, the loss of cellular integrity in combination with edema and hemorrhage contributes to an increased distribution volume in the area of MI. This area will appear hyperenhanced when examined by DE-MRI. As the MI heals, the necrotic tissue is replaced by scar tissue.[132] The scar tissue also has a larger distribution volume than the viable myocardium. Hence, an increase in distribution volume can also explain why myocardial scar tissue is hyperenhanced when examined by DE-MRI.

It is still controversial whether or not non-infarcted myocardium in the peri-infarction zone can appear hyperenhanced early after acute MI. Some have suggested that only irreversibly injured myocardium hyperenhances even early after MI.[134] Others maintain that reversibly injured myocardium in the periinfarction
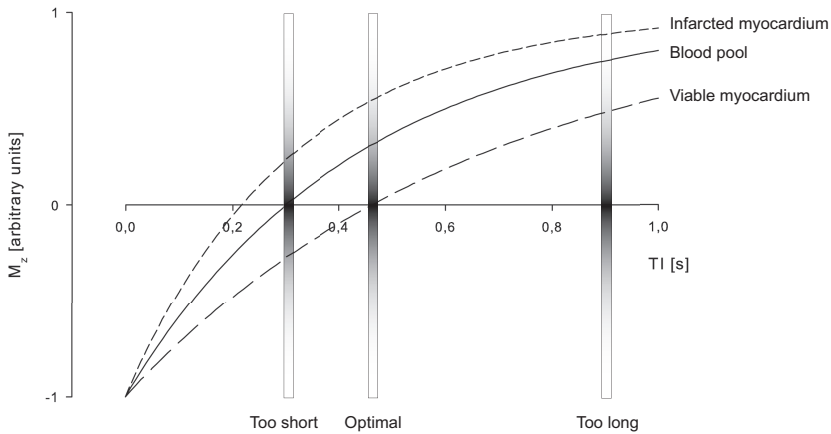
FIGURE 1.2 T1-relaxation curves for infarcted and viable myocardium as well as for the blood pool after administration of a gadolinium-based contrast agent, adapted from Hedstrom *et al.*[133] There is a larger distribution volume for the contrast agent in the infarcted myocardium as compared with the viable myocardium and the blood pool. Thus, the infarcted myocardium has a shorter T1 and a faster recovery of the longitudinal magnetization M_z (the component of M in the direction of the main magnetic field, B). By choosing the optimal TI, the signal from the viable myocardium is nulled and this part of the myocardium appears black. If the TI is too short or too long, the relative contrast between viable and infarction myocardium is reduced or lost. The signal intensity ranges from 0 to ± 1, where 0 equals black and + or -1 equals white.

zone can appear hyperenhanced early after MI, contributing to a slight overestimation of the acute MI size.[135–139] This issue is further discussed in the appended Paper III.

1.3   Electrocardiography in ischemic heart disease

The 12-lead ECG is probably still the most frequently used diagnostic method in patients with suspected IHD. All patients presenting at the emergency room with chest pain have an ECG recorded to exclude or confirm ongoing myocardial ischemia. There are several reasons for the frequent use of ECG as a diagnostic

method. First, it is an inexpensive examination which can be performed within a few minutes. Second, the technique is widely available, even in the developing parts of the world. Finally, the medical society has a long experience with the method since it has been around for more than 100 years.

The following section highlights some of the important milestones in the development of the ECG technique and our current understanding of the cardiac electrical properties.

The history of ECG: Important milestones

The development of electrocardiography has been driven both by biological discoveries and pioneering engineering in the field of electromechanics. One of the earliest observations of cardiac electricity was made in 1775 by Peter Christian Abildgaard[140] who showed that the pulse could be restored in lifeless hens by applying electrical shocks across the chest: "With a shock to the head, the animal was rendered lifeless, and arose with a second shock to the chest; however, after the experiment was repeated rather often, the hen was completely stunned, walked with some difficulty, and did not eat for a day and night; then later it was very well and even laid an egg."

In 1791, the Italian anatomist Luigi Galvani was the first to describe the electrical activity in living tissue by experiments on frogs.[141] Galvani's name is the origin of the "galvanometer" which is an instrument by which electricity can be measured and recorded. The current ECG recorders are in fact very sensitive galvanometers.

In 1878, the British physiologist John Burdon Sanderson was the first to record cardiac electrical currents with a capillary electrometer.[142] He showed that the cardiac electrical impulse consisted of two phases (later called QRS and T).

In 1889, the British physiologist Augustus D. Waller published the first human ECG.[143]

In 1895, the Dutch physiologist Willem Einthoven, inspired by Waller, distinguished five deflections in the ECG which he named P,Q,R,S, and T.[144] The choice of P is a mathematical convention by using letters from the second half of the alphabet. N has other meanings in mathematics and O is used for the origin of the Cartesian coordinates. P is simply the next letter, followed by QRS and T.

In 1902, Einthoven recorded the first ECG with a string galvanometer, which was a development of the galvanometer, capable of detecting very weak electrical currents. In 1906, Einthoven published the first structured report on normal and abnormal ECG findings, including among others ventricular and atrial hypertrophy, notching of the QRS complex, ventricular premature beats, atrial flutter, and AV block.[145]

In 1920, the American Harold Pardee published the first ECG in a patient

suffering from acute myocardial ischemia: "T waves are tall and start from a point well up on the descent of the R wave.".[146]

In 1924, Willem Einthoven received the Nobel Prize in medicine or physiology for inventing the electrocardiograph. In 1934, Frank Wilson and coworkers describes "Wilson Central Terminal" for the first time.[147] By connecting the limb leads I, II, and III, they defined an indifferent electrode (the Wilson Central Terminal) which acts as the negative pole for "unipolar leads" that can be placed anywhere on the body surface. The "unipolar lead" was given the prefix "V" for the voltage measured at the site of the electrode. This is the origin for the names of the precordial leads V1-V6 used today in recording of the standard 12-lead ECG. The term "unipolar lead" is actually misleading since the potential difference must be measured between two points.

In 1938, a standardization of the precordial leads was suggested and the leads V1-V6 were described as we know them today.[148] The standardization of placement of the precordial leads was a committee decision, made with the specific intent of standardizing research.

In 1942, Emanuel Goldberger introduced the augmented limb leads aVR, aVL, and aVF.[149] The augmented leads have 50% higher amplitude than the original Wilson leads VR, VL, and VF, which had the Wilson Central Terminal as negative pole.

In 1949, Jeff Holter published the first results from experience with a portable ECG recording device capable of monitoring and transmitting ECG signals.[150] The first Holter Monitor weighed 75 pounds and was carried as a backpack.

In 1958, Professor Åke Senning implanted the first cardiac pacemaker designed by Rune Elmqvist. The recipient was a 43-year old patient suffering from atrioventricular block and syncope.

In 1970, Dirk Durrer and co-workers published a description of the complete cardiac electrical activation sequence in humans.[151] To obtain the time course and instantaneous distribution of the activation of the human heart, isolated hearts from seven patients who died from various cerebral conditions and had no history of cardiac disease were examined. The electrical activity was recorded at the epicardial surface and throughout the transmurality of the muscle wall by use of multipoint intramural plunge electrode mapping. In total, activation information was collected from 870 electrode terminals in each heart.

There has been a lot of technical advances that have resulted in the ECG recorders used today, which will not be covered by this section.

ECG and ischemia

As mentioned above, in conjunction with the ischemic cascade, signs of acute ischemia can be seen in the ECG due to alterations of the electrical properties

in ischemic myocardium. The ischemia causes repolarization abnormalities in the ischemic myocardium which alters the ST segment. The ST segment in a lead overlaying the ischemic myocardium can be either elevated or depressed. There are different pathophysiological explanations for this ST-elevation and ST-depression. Let us take a closer look at the repolarization abnormalities associated with myocardial ischemia.

Diastolic and systolic injury currents

Under normal conditions the ST segment is an approximately isoelectrical baseline. As previously mentioned ischemia can reduce the resting membrane potential, shorten the duration of the action potential, and reduce the amplitude of the action potential plateau phase. These alterations of the electrical properties in ischemic myocardium result in a voltage gradient between normal and ischemic myocardium. The voltage gradient induces an injury current, seen as deviation of the ST segment on the body surface ECG. It has been shown that these injury currents arise in the border zones between normal and ischemic myocardium.[15]

There are two types of injury currents, a diastolic injury current and a systolic injury current. The diastolic injury current causes a negative displacement (depression) of the diastolic baseline due to a reduced resting membrane potential. This can partly be explained by leakage of intracellular K^+ in the ischemic myocytes.[152] As a result, a lead overlaying the ischemic myocardium will detect a negative deflection during electrical diastole. Thus, no ST-segment elevation is detected by this lead. Still, the classical sign of acute ischemia is ST-segment elevation in an overlying lead. The ST-segment elevation is thereby a result of the ECG recorder's inability to compensate for baseline shifts. Hence, when the diastolic baseline drops the ECG recorder shifts the baseline to its original position and the result is an elevation of the electrical systolic segment, the ST segment.

There is, however, evidence suggesting that ST-segment elevation can also originate from a true elevation of the ST segment caused by systolic injury currents. The shortening and decrease in amplitude of the action potential causes the injury current to flow during the electrical systole and cause ST-segment elevation and sometimes hyperacute tall T waves.[40]

If the ischemia is transmural the overall ST vector is directed toward an overlying lead which then shows ST-segment elevation. When ischemia is subendocardial, however, the ST vector is typically shifted towards the endocardial layers and the ventricular cavity, resulting in an ST depression in an overlaying lead. Moreover, transmural ischemia does not necessary equate to ST-segment elevation. The direction of the ST deviation also depends on the lead position in relation to the over all ST-segment vector. For example, if the posterolateral LV wall is subject to transmural ischemia the main finding in the standard 12-lead ECG is ST-segment

depression in lead V1 and V2.[153] This is because the ST vector is directed away from the the positive poles of V1 and V2. Thus, this ST-segment depression should be considered indicative of transmural ischemia.

ECG and infarction

As previously discussed, a possible consequence of myocardial ischemic is myocyte death, MI. Therefore, one of the reasons why injury currents resolve is the development of MI. Hence, the remaining ECG abnormalities are not due to injury currents, but rather to the established MI. The MI will affect the local activation sources of the myocardium, seen as deviation of the QRS waveforms away from an electrode overlaying the infarcted area. The MI might also cause persistent alteration of the myocardial repolarization, resulting in remaining T wave alterations.[154] The QRS complex is altered to a variable degree, in variable leads depending on the size, location and morphology of the MI. As previously discussed the extent of MI is dependent on which vessel is occluded. The myocardial activation (depolarization) vector is a resultant of all parts of the myocardium that are depolarized at a given time point. The result of the time resolved propagation of the depolarization vector during one cardiac cycle is what causes the deflections of the QRS complex seen in different leads. Regions of MI will influence the normal depolarization vector according to the size, location and morphology of the MI. If the initial depolarization forces are directed away from an overlaying lead, then the initial QRS deflection in that lead will be negative, resulting in a Q wave. Thus, presence of Q waves can be a sign of MI. Previously, it was thought that the MI had to be transmural in order to cause pathological Q waves.[155] This association has later been rejected.[156–162] Given that the first part of the QRS complex reflects depolarization of subendocardial myocardium, endocardial extent of MI is likely to be a determinant of pathological Q waves. This is discussed in the appended Paper II.

Infarction can result in other changes in the QRS complex than pathological Q waves. If the MI is isolated to the posterolateral LV wall, then the alterations in the QRS complex are not Q waves but rather prominent R waves in leads V1 and V2. In fact, 8-10 % of all MIs are limited to the basal parts of the LV and thereby cannot produce Q waves.[163]

By knowing which parts of the myocardium that normally depolarize at which time, it is possible to derive information about which parts that do not depolarize based on alterations of the QRS complex. Thus, alterations of the QRS complex have the potential to provide information about MI size, location and morphology. This has been utilized by Ronald H. Selvester, who pioneered the Selvester QRS scoring system.[164]
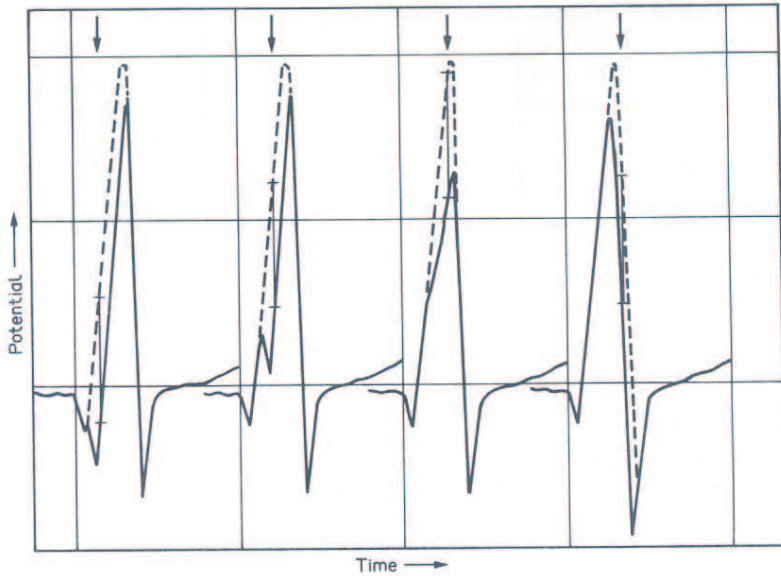
FIGURE 1.3 The QRS complexes represent the simulated lead V6 after adding a small MI (15 x 7 mm) at various levels in the junction of the inferior and the posteroapical LV segments in the propagation model of the heart. The dotted lines in each QRS complex represents the normal activation seen in lead V6 without MI. To the left, the MI is placed in the endocardium and in each of the following complexes the center of the MI is moved 2.5 mm towards the epicardium. The vertical arrows represent the time when the activation front passes the center of the MI in each instance. In the first case, abnormal Q waves were produced only by a very strategically placed MI. Notched R, attenuated peak R, or changes in the R:S-amplitude ratio are equally valid markers of MI in the LV wall. In basal segments in general, and in midventricular posterolateral segments, which are activated in the mid- to late part of the QRS complex, only mid to late QRS changes will result even from extensive MI. Reproduced from "Selvester RH, Wagner GS, and Ideker RE. Myocardial infarction. In Macfarlane PW and Lawrie TDV, editors, *Comprehensive electrocardiology: Theory and practice in health and disease*, volume 1, page 574. Pergamon press, New York, 1st edition, 1989" with permission from Elsevier.

The Selvester QRS scoring system

Based on the description of the human myocardial activation by Durrer *et al*,[151] Selvester and co-workers designed a computer simulation of the human activation sequence. The computer simulation was based on a 1-mm grid propagation model and used the 12-segment subdivision of the LV described in Figure 1.4. The computer model included a realistic simulation of an inhomogeneous volume conductor including cardiac blood, myocardium, and lungs to mimic an adult male torso. Thus, it was possible to obtain different patterns of QRS changes on a fictive torso surface by simulating MI of different sizes at different locations in the LV. Figure 1.3 shows how the QRS complex is influenced by simulation of MI at different places throughout the thickness of the LV wall. The results from the computer simulations were used for developing the Selvester QRS scoring system.

In order to assess the diagnostic ability of the QRS scoring system, derived from the computer simulations, the system had to be validated in humans. Galen S. Wagner and associates were responsible for this validation process. The first step was to make the QRS scoring procedure easy to perform and develop a way to display the results in an intuitively manner. The specificity and inter- as well as intra-observer variability of the QRS scoring system was evaluated in 1982.[164] The QRS scoring system was then systematically evaluated in human postmortem histopathology studies of single infarcts located in the anterior,[41] inferior,[43] and posterolateral[42] parts of the LV wall.

The correlation between QRS score and MI size by histopathology was strong for all locations of MI (R values ranging from 0.72-0.80). QRS scoring of the ECG recorded at hospital discharge in patients with acute MI has been shown to have prognostic value for patient outcome.[165] Furthermore, a higher QRS score is associated with a higher mortality in patients with documented coronary artery disease.[166] The scoring system has also been proven useful for predicting recovery of LV function after acute MI.[167, 168] Furthermore, the Selvester QRS scoring system has been used for screening of non-acute MI utilizing a subset of the QRS criteria (Q=30 ms in aVF, R=10 ms or R=0.1mV in V2, and R=40ms in V2). Using these QRS criteria, it was possible to identify single, non-acute anterior and inferior MI in 80% of the patients, and falsely indicating presence of MI in only 5% of normal subjects.[169]

The 50-criteria, 31-point Selvester QRS scoring system used today[170, 171] is based on a quantitative evaluation of 10 of the 12 standard ECG leads. It enables estimation of global MI size as well as MI distribution into 12 LV segments (Figure 1.4).

QRS score has been shown to decrease over time after acute MI.[48, 49] Until recently, however, it has been difficult to establish the anatomic correlate of these changes due to lack of an accurate in vivo method for MI visualization. This
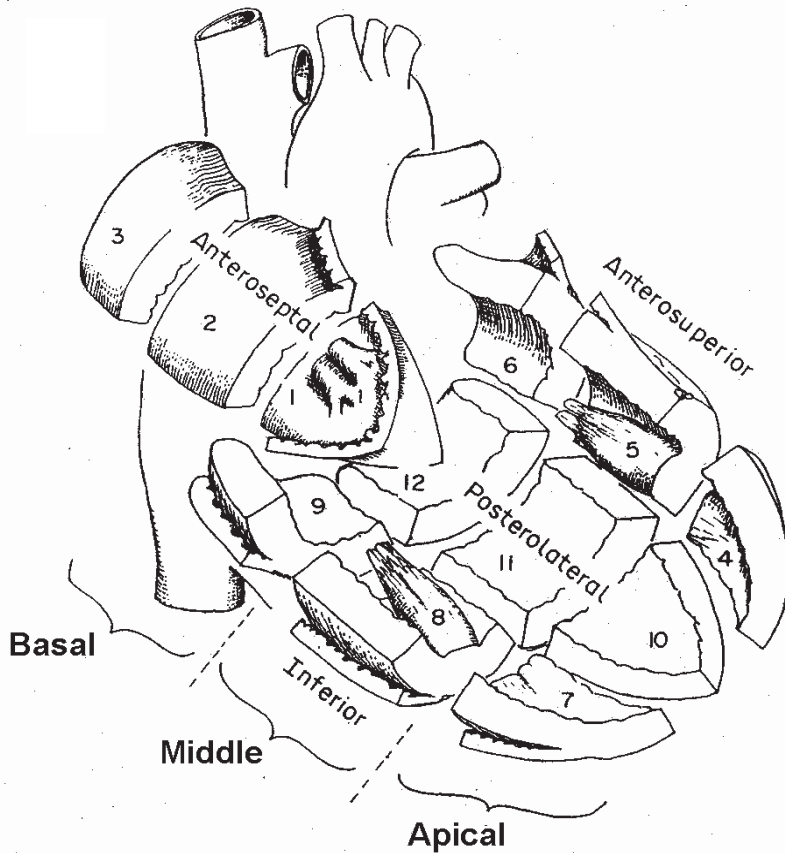
FIGURE 1.4 Subdivision of the left ventricle into 12 segments. The 12-segment model is used for describing the local MI extension by the Selvester QRS scoring system. In paper I and IV the regional MI extent assessed by DE-MRI was performed according this 12-segment model. Reproduced from "Selvester RH, Wagner GS, and Ideker RE. Myocardial infarction. In Macfarlane PW and Lawrie TDV, editors, *Comprehensive electrocardiology: Theory and practice in health and disease*, volume 1, page 567. Pergamon press, New York, 1st edition, 1989" with permission from Elsevier.

correlation can now be studied using DE-MRI. As discussed above, DE-MRI can be used to depict MI in vivo with great accuracy. Hence, it is possible to evaluate the performance of the Selvester QRS scoring system using an imaging technique rather than histopathology. The first studies comparing QRS score and MI size assessed by DE-MRI are the appended Papers I-IV.

The Selvester QRS scoring system is limited to patients with normal cardiac conduction except for the MI-related QRS changes. Bundle branch block, fascicular block, preexcitation and conduction abnormalities due to ventricular hypertrophy are all confounding factors for QRS scoring. Howe and coworkers[172] showed that right ventricular hypertrophy reduced the diagnostic accuracy of the QRS scoring system significantly. Freye and coworkers[173] showed that LV hypertrophy was a significant confounding factor for QRS scoring and suggested a modified scoring system in the presence of this confounder. Furthermore, multiple MIs might cause problems for the QRS scoring. Due to so called cancellation effects, ECG changes due to anterior and inferior MI can counter balance each other and result in no or only minor changes in the QRS complex.[174, 175] Also, age and sex are potential confounding factors for the QRS scoring since amplitudes and durations of the QRS wave forms change with age and differ between sexes.[176] In fact, age and sex have been shown to affect the diagnostic accuracy of the Selvester QRS scoring system.[177] Age- and sex-specific criteria have been proposed[178] but need to be further evaluated.

Chapter 2

Aims of the Work

The general aim of this thesis was to further elucidate the relationship between MI characteristics and infarct-related changes in the QRS complex.

The standard 12-lead ECG is used clinically to characterize MI. Q waves are still equated with transmural MI by many physicians, despite that Q waves might develop in conjunction with non-transmural MI.

Furthermore, the relationship between findings on the body-surface ECG and MI characteristics during MI healing has not yet been studied.

Therefore, we sought to explore this relationship shortly after acute MI, during MI healing, and in healed MI to reveal the pathophysiologic basis for Q waves and to determine how changes in MI characteristics over time are reflected in the 12-lead ECG.

The specific aim for each paper was:

I. To test the hypotheses that QRS score is related to MI size and transmurality and that presence of Q waves should not be equated to transmural MI in patients with reperfused first-time MI.

II. To test the hypothesis that the endocardial extent of MI is a stronger predictor of presence of Q waves than is MI transmurality, and to explore the relationship between QRS score and different MI characteristics in patients with reperfused first-time MI.

III. To explore the changes in hyperenhanced myocardium, recovery of global and regional LV function, and sequential ECG changes at multiple points in time during the first year after MI in patients with reperfused first-time MI.

IV. To evaluate the Selvester QRS scoring system for quantifying regional and global MI size in patients with chronic ischemic heart disease and old anterior MI.

Chapter 3

Materials and Methods

3.1 Study populations

All protocols and procedures were approved by the ethics committee for human research at Lund University, Sweden. Patients included in Paper I-III were prospectively recruited at the Lund University Hospital, Lund, Sweden. Patients included in Paper IV were retrospectively enrolled at the Cleveland Clinic Foundation, Cleveland, Ohio, USA, or at the Lund University Hospital, Lund, Sweden. All patients gave their written informed consent to participate in the respective study.

Paper I & II

All patients included in Paper I and II had clinical, biochemical, and electrocardiographic signs of acute MI. All patients underwent successful percutaneous coronary intervention (PCI) with stenting. Exclusion criteria comprised history of prior MI, contraindications for MRI, and ECG confounding factors such as bundle branch block or fascicular block.

Paper III

For paper III, patients arriving at the Coronary Care Unit of Lund University Hospital with first-time MI between May, 2000 and March 2005 were prospectively enrolled. All patients had clinical, biochemical, and electrocardiographic signs of acute MI. All patients included underwent successful percutaneous coronary intervention (PCI) with stenting. In conjunction with the PTCA the patients received a platelet glycoprotein IIb/IIIa inhibitor. Patients with a known prior MI or angiographic signs of collateral flow supplying the occluded vessel

and those who had reinfarction or coronary intervention during the follow-up were excluded. Patients with contraindications for MRI were also excluded.

Paper IV

Patients in Paper IV were retrospectively included by reviewing the reports for patients with chronic ischemic heart disease clinically referred for viability assessment using DE-MRI at the Section of Cardiovascular Imaging, Cleveland Clinic or at Lund University Hospital between 1998 and 2001. Patients included had single anterior MI established by DE-MRI and a standard 12-lead ECG recorded within two months of the MR examination. Exclusion criteria comprised ECG confounding factors and re-infarction or coronary interventions during the time between the MR examination and the recording of the ECG.

3.2 Assessment of cardiac function using cine MRI

MR imaging

All imaging was performed in relation to the spatial orientation of the LV long axis.[121] Long- and short-axis images were acquired using a 1.5T MR system (Siemens Magnetom Vision, or Philips Intera CV). The cine images were obtained by using either a cine gradient recalled-echo (GRE) sequence (Siemens) or a steady state free precession (SSFP) sequence (Philips). The cine GRE sequence was prospectively ECG-triggered and generated images with the following typical image parameters: spatial resolution $1.6 \times 1.6 \times 8$ mm, slice gap 2mm and temporal resolution 50 ms. The cine SSFP sequence was retrospectively ECG-gated and generated images with the following typical image parameters: spatial resolution $1.25 \times 1.25 \times 8$ mm, no slice gap, temporal resolution 33 ms and SENSE factor 2.

Image analysis

Global left ventricular function

All functional analyses were obtained from the short-axis cine images covering the LV. Left ventricular mass (LVM), LV end-diastolic volume (EDV), and LV end-systolic volume (ESV) were determined by manually tracing the endocardial and epicardial borders of the LV myocardium both in end-diastole and end-systole according to established methods.[179] The LV stroke volume (SV) was calculated as EDV-ESV and the LV ejection fraction was calculated as SV / EDV. Papillary muscles were included as a part of the LV muscle wall.

Regional wall thickening

In paper III, the regional wall thickening was determined in a 72-segment LV model previously described.[54] After manually tracing of the endocardial and epicardial borders, the regional wall thickening was calculated as the percent change in radial wall thickness between end-diastole and end-systole. For the wall thickening analysis the papillary muscles were excluded from the muscle wall. The end-diastolic and end-systolic wall thickness was determined using a centerline approach, assessing the radial wall thickness at each 4.5 degrees around the short-axis of the LV.

3.3   Infarct quantification by DE-MRI

MR imaging

For MI visualization, imaging was performed in the corresponding long- and short-axis planes as for the cine images, using an inversion recovery turbo fast low-angle shot sequence.[180] Images were acquired in late diastole during breath-hold either with a two dimensional (Siemens) or a three dimensional (Philips) approach. Image parameters for the two dimensional image acquisition were: signal sampling ever other heart beat, spatial resolution 1.6*x*1.6*x*8mm and slice gap 2mm. Image parameters for the three dimensional approach were as follows: signal sampling every heart beat, spatial resolution 1.6*x*1.6*x*8mm and no slice gap. With both approaches, the TI was manually adjusted to null the signal from non-infarcted myocardium. Twenty to 40 minutes prior to image acquisition, a Gd-based contrast agent (Gd-DOTA or Gd-DTPA) was administered intravenously (0.2 mmol/kg body weight). Since both acute infarcted myocardium and the healed myocardial scar have a greater tissue distribution volume compared to viable myocardium, these regions will appear hyperenhanced in relation to viable myocardium.

Image analysis

Global infarct characteristics

The quantification of the hyperenhanced tissue was performed on the DE-MRI short-axis images. The region of hyperenhancement in each short-axis slice was manually (Paper I and IV) or semi-automatically (Paper II and III)[181] traced (Figure 3.1A). The absolute MI size in ml was calculated by multiplying the total area of MI by the slice thickness. The relative MI size in percent was defined as MI volume / LVM volume.

The mean MI transmurality was determined by measuring the transmural extent of hyperenhancement at each 4.5 degrees around the short-axis images using a centerline approach (Figure 3.1B).

The endocardial extent of MI was determined by measuring the circumferential extent of hyperenhancement in each short-axis slice (Figure 3.1C). The circumferential extent was then multiplied by the slice thickness to obtain the total endocardial surface area containing MI (Figure 3.1D). The endocardial extent of MI was expressed as a percentage of the total endocardial surface.

Regional infarct characteristics

In paper IV, the amount of hyperenhanced myocardium was determined for each of the 12 LV segments used in the Selvester QRS scoring system (Figure 1.4). To obtain a similar 12-segment model for the DE-MRI description of the MI, each short-axis slice was divided into the four quadrants and the short-axis slices were divided into basal, middle apical slices corresponding to Figure 1.4.

In Paper I, the transmural extent of hyperenhancement was determined for the 12 LV segments described above. In Paper III, the regional transmurality was determined in the corresponding 72 LV segments as for the regional wall thickening analysis.
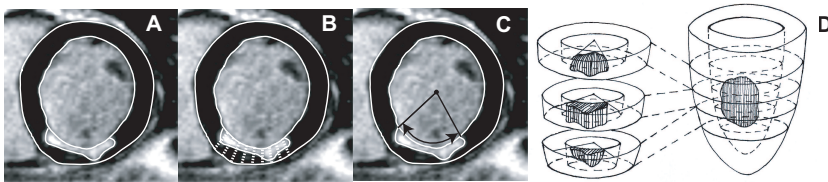

FIGURE 3.1 Definition of the different MI characteristics illustrated in one DE-MRI short-axis image. **A**) Infarct size determined by delineation of the MI borders in each short-axis image. **B**) Mean MI transmurality defined as the average transmurality measured at each $4.5°$ from the center of the LV blood pool. **C**) Endocardial circumferential extent of MI for one short-axis image. **D**) The total endocardial extent of MI defined as the endocardial surface being infarcted. The infarcted endocardial surface was calculated as the product of slice thickness and circumferential extent of MI for each short-axis slice.

3.4   Infarct quantification by ECG

The ECGs that were subject to analysis were recorded with a frequency response set at the range of 0.05 to 150Hz, and the sampling rate was 500Hz. The paper speed was set set at 50mm/s (Paper I-III) or 25mm/s (Paper IV).

The Selvester QRS scoring system

Figure 3.2 shows the 50-criteria, 31-point Selvester QRS scoring system. This system (used in Paper I-IV) is used to estimate global and local MI size as well as regional transmurality based on infarct-related QRS changes in lead aVL, I, II, aVF, and V1-V6. In addition, V1 and V2 are also considered for detecting and quantifying posterolateral MIs. Q-, R-, and S-wave amplitudes, Q- and R-wave durations, and R:Q- and R:S-amplitude ratios are considered according to the criteria in Figure 3.2, Panel A. Each QRS point awarded in Panel A is considered to represent infarction in approximately three percent of the LV. Each criterion is weighted according to the estimated amount of MI that causes the criteria to be met. The summed QRS points multiplied by 3 constitutes the global QRS score which represents the estimated relative MI size. For example, in lead aVF QRS points can be awarded for Q-wave duration or R:Q-amplitude ratio. If the duration of the Q wave is 50ms or longer, three QRS points are awarded; whereas if the Q wave duration is 30ms, only one point is awarded. If the R:Q-amplitude ratio in the same lead is ≤1, an additional two QRS points are awarded. Thus, lead aVF can generate a maximum of five QRS points, representing an estimated relative MI size of 15%.

The Selvester QRS scoring system was previously based on 54 criteria, capable of generating 32 QRS points. However, Sevilla et al[175] showed that four of the 54 criteria (notched R wave in V4-V6, and S wave in V1 ≥1.8mV) did not provide additional information about infarcted myocardium; therefore, these four criteria were later excluded from the scoring system.[161, 170, 171]

As shown in Figure 3.2, Panel B, the Selvester QRS scoring system also provides an estimate of the distribution of the MI into 12 LV segments (Figure 1.4) based on the QRS changes. For each QRS point awarded in Panel A, three points are distributed into the 12 segments of the LV. Thus, by distributing the points awarded in Panel A into Panel B, an estimate of the MI distribution into the 12 LV segments is obtained. This estimate of the regional amount of MI is referred to as the local QRS score.

For accurate QRS scoring, it is fundamental to have rigorous definitions of the different waveforms in the QRS complex. If the initial deflection in the QRS complex is negative, a Q wave is present. The Q wave can be either smooth or "notched". The Q wave is smooth if the initial negative deflection has no

Panel A			Panel B Ant-sep 1 2 3	Ant-sup 4 5 6	Inf 7 8 9	Post-lat 10 11 12
Lead	**Criteria**	**Pts.**				
I [1]	Q ≥ 30 ms	1		1 1		1
	R/Q ≤ 1	1		1 1 1		
	R ≤ 0.2 mV	1		1 1 1		
II [2]	Q ≥ 40 ms	2			1 2 2	1
	Q ≥ 30 ms	1			1 1	1
aVL [2]	Q ≥ 30 ms	1		2 1		
	R/Q ≤ 1	1		1 2		
aVF [5]	Q ≥ 50 ms	3			3 2 2	1 1
	Q ≥ 40 ms	2			2 2 2	
	Q ≥ 30 ms	1			2 1	
	R/Q ≤ 1	2			2 3	1
	R/Q ≤ 2	1			2	
V1(ant) [1]	Any Q	1	1 2			
(post) [4]	R/S ≥ 1	1				1 1 1
	R ≥ 50 ms	2			1 1	2 2
	R ≥ 1.0 mV	2			1 1	2 2
	R ≥ 40 ms	1			1	2 1
	R ≥ 0.6 mV	1			1	1 1
	Q and S ≤ 0.3 mV	1				1 1
V2(ant) [1]	Any Q	1	1 1 1			
	R < RV1	1	1 1 1			
	R ≤ 10 ms	1	1 1 1			
	R ≤ 0.1 mV	1	1 1 1			
(post) [4]	R/S ≥ 1.5	1			1	1 1
	R ≥ 60 ms	2			1 1	1 2 1
	R ≥ 2.0 mV	2			1 1	1 2 1
	R ≥ 50 ms	1			1	1 1
	R ≥ 1.5 mV	1			1	1 1
	Q and S ≤ 0.4 mV	1			1	1 1
V3 [1]	Any Q	1	1 1	1		
	R ≤ 20 ms	1	1 1	1		
	R ≤ 0.2 mV	1	1 1	1		
V4 [3]	Q ≥ 20 ms	1	1 1	1		
	R/Q ≤ 0.5	2	2 2	1 1		
	R/S ≤ 0.5	2	2 2	1 1		
	R/Q ≤ 1	1	1 1	1		
	R/S ≤ 1	1	1 1	1		
	R ≤ 0.7 mV	1	1 1	1		
V5 [3]	Q ≥ 30 ms	1	1 1	1		
	R/Q ≤ 1	2	2 1	2 1		
	R/S ≤ 1	2	2 1	2 1		
	R/Q ≤ 2	1	1	1 1		
	R/S ≤ 2	1	1	1 1		
	R ≤ 0.7 mV	1	1	1		
V6 [3]	Q ≥ 30 ms	1		1	1	1
	R/Q ≤ 1	2	1	1	1	2
	R/S ≤ 1	2	1	1	2	2
	R/Q ≤ 3	1		1	1	1
	R/S ≤ 3	1		1	1	1
	R ≤ 0.6 mV	1		1	1	1
Total score:						
Total score per region:						

FIGURE 3.2 The 50-criteria, 31-point Selvester QRS-scoring system. **Panel A:** The 50 QRS criteria and their corresponding points. If two or more criteria within the same box are met, only the criterion generating the highest number of points is considered. Under each lead the maximum lead score is seen within parenthesis. **Panel B:** Distribution of QRS points awarded in Panel A into local QRS points of the 12 LV segments. A total score of 8 in a segment was considered 100% MI, since each segment represents approximately 8% (1/12) of the LV. Ant indicates anterior; Ant-sep, anteroseptal; Ant-sup, anterosuperior; Inf, inferior; LV, left ventricle; ms, milliseconds; mV, millivolts; post, posterior; Post-lat, posterolateral; Pts., points)

reversal in direction of $\geq$0.05mV preceding the next positive deflection in the QRS complex (Figure 3.3, upper panel). A "notched" Q wave is present when there is any reversal in direction of $\geq$0.05mV before returning to the baseline (Figure 3.3, lower panel). This has implications for the measurements of the Q-wave duration and amplitude. If the Q wave is smooth, the Q-wave duration and amplitude is measured as the width and height of the entire initial negative deflection. When the Q wave is "notched", however, the Q-wave duration is measured along the PQ baseline as the width from the beginning of the initial negative deflection to the point just above the peak of the notch (Figure 3.3, lower panel). The amplitude of the "notched" Q wave is defined as the amplitude measured from the PQ baseline to the nadir of the negative deflection preceding the notch.

An R wave is present when the initial deflection of the QRS complex is positive or if a positive deflection is found after an initial Q wave. It extends until it completes the QRS complex or until it becomes an S wave.

If no persistent ST-segment deviation is present, the PQ baseline and the ST baseline are isoelectric and the amplitudes of the waveforms can be measured from either baseline. However, sometimes injury currents remain for a prolonged period of time, resulting in incomplete resolution of the ST-segment deviation. The Q- and R-wave amplitudes should then be measured from the PQ baseline and the S-wave amplitude should be measured from the J point of the ST segment.

In spite of rigorous waveform definitions and accurate waveform measurements, manual QRS scoring is associated with inter-observer variability. Also, the manual scoring is laborious and time consuming, especially for the untrained scorer. It has previously been shown the automated computerized scoring algorithms are superior to manual scoring, both for duration and amplitude measurements.[177, 182, 183] These automated approaches have, however, had a limited clinical use because of the incompatibility with commercially available ECG analysis software. More recently, a novel automated QRS scoring algorithm was proposed and validated against consensus measurements of expert electrocardiologists.[171] This novel approach has potential for clinical implementation since it can easily be incorporated into commercially available ECG analysis software.

To refine QRS criteria of MI, a non-ECG method for MI characterization is needed. Since DE-MRI can be used to depict MI non-invasively, this technique can play an important role in future refinement of QRS criteria and for optimization of automated QRS scoring algorithms.

Minnesota coding

In Paper II, the presence of infarct-related Q waves was determined using Minnesota coding.[184] Minnesota coding is a coding scheme used for standardization
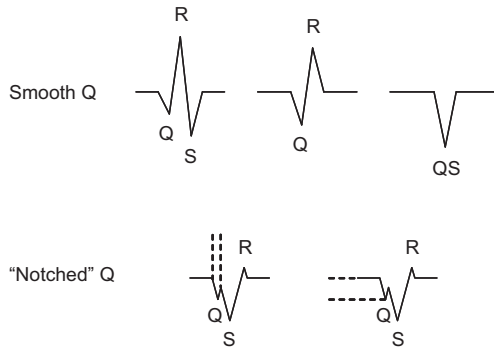
FIGURE 3.3 Q wave definition for QRS scoring. **The upper panel** shows examples of smooth Q waves. For the smooth Q waves there is no reversal in direction of $\geq$0.05mV preceding the return to the baseline. The Q-wave duration and amplitude is measured as the width and height of the entire initial negative deflection. **The lower panel** shows how the Q-wave duration and amplitude is measured when a "notched" Q wave is present. The Q wave is "notched" when there is a reversal in direction of $\geq$0.05mV before returning to the baseline. The dashed lines indicate how Q-wave duration and amplitude are defined. Q-wave duration is measured along the PQ baseline as the width from the beginning of the initial negative deflection to the point just above the peak of the notch. The Q-wave amplitude is measured as the amplitude from the PQ baseline to the nadir of the negative deflection preceding the notch.

of ECG wave form classification. Q and QS patterns can be classified as being more or less indicative of MI. By classifying the patient's ECG according to the Minnesota coding, patients were classified as having Q-wave MI (Minnesota code 1–1 to 1–3) or non-Q-wave MI. The Minnesota coding also provides a suggestion of MI location based on in which leads the Q waves are found.

3.5 Statistical analyses

Data are presented as mean $\pm$ standard deviation unless otherwise is specified. A P-value of < 0.05 was considered indicative of statistical significance throughout

the statistical analyses.

To assess the correlation between different variables, linear regression analysis was performed using the Pearson correlation coefficient for normally distributed data and Spearman's rho when the data was not normally distributed. For normally distributed data, paired and non-paired t-tests were used to assess variance between data. To assess variance between data not normally distributed, the Mann-Whitney test and the Wilcoxon signed-rank test were used. To show differences in measurements between two methods, Bland-Altman plots with the data by the reference method on the horizontal axis, were used.

In Paper I, the Jonckheere-Terpstra test for trend was used to assess the relationship between local QRS score and MI transmurality by DE-MRI in the 12 LV segments.

In Paper II, univariate and multivariate logistic regression analysis were performed to identify independent predictors of the presence of Q waves. In this paper, Kappa statistics was used to assess the agreement between the ECG indices and DE-MRI with regard to MI location.

In Paper III, a linear mixed-effects model was used both to assess the trend of regional wall thickening with increasing transmural extent of hyperenhancement and to assess differences in wall thickening over time within the different LV segment groups. Mixed-effect modeling was used for the segmental analysis, given the dependence of multiple segments per patient.

In Paper IV, the diagnostic performance of the QRS scoring system was assessed using receiver operating characteristic (ROC) curves.

Chapter 4

Results and Comments

4.1 QRS score and Q waves versus infarct transmurality (Paper I)

The ability of the 12-lead ECG to quantify size and transmural extent of MI has not been fully explored. Q waves are still thought of as indicative of transmural MI, despite previous studies which have rejected this association.[159, 160] We hypothesized that size and transmural extent of acute MI indeed can be estimated by QRS scoring on the 12-lead ECG using delayed contrast-enhanced magnetic resonance imaging (DE-MRI) as gold standard and that Q waves are not predictive of transmural MI.

Figure 4.1A shows that there is a significant relationship between global QRS score and MI size. Figure 4.1B demonstrates that local QRS score increases progressively as the regional MI transmurality (P_{trend}<0.001).

In Figure 4.2 the patients were categorized according to MI transmurality. There was no significant difference in the number of Q-wave related QRS points awarded between patients with transmural and non-transmural MI. Thus, Q waves cannot be considered indicative of transmural MI.

The concept that Q-wave MI should be equated to transmural MI originates from a study by Prinzmetal et al[155] in 1954. They concluded from their pathology studies that only transmural MI could give rise to pathologic Q waves in the 12-lead ECG. However, more recent litterature has rejected the notion that Q waves can be used to differentiate transmural from non-transmural MI.[156–158] Furthermore, studies in patients with first-time MI have not been able to show any differences in clinical outcome between Q-wave and non-Q-wave MI.[185–187] Pathological Q waves only appear when the MI causes the initial depolarization forces to be directed away from the leads in which the Q waves are seen, whether
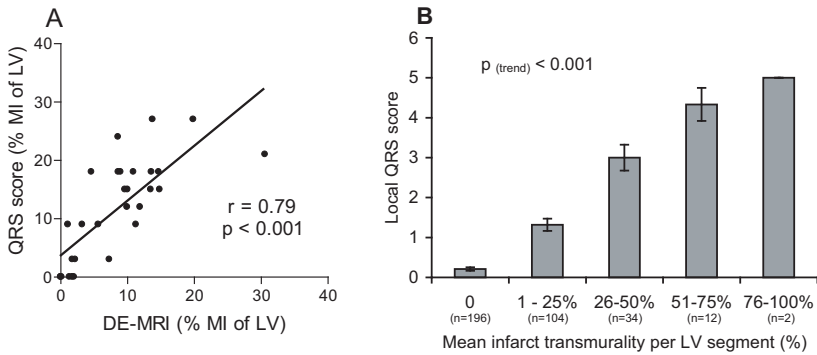
FIGURE 4.1 The relationship between infarct size by QRS scoring and DE-MRI (**A**) and the relationship between local QRS score and mean MI transmurality by DE-MRI in the 12 LV segments (**B**). The local QRS score increased progressively as infarct transmurality increased. Bars indicate mean local QRS score $\pm$ standard error of the mean for different ranges of MI transmurality.

the MI is transmural or not. Eight to ten percent of the MIs in general involve only the base of the LV and do not produce initial QRS changes.[163] Thus, changes in the later part of the QRS complex must also be taken into consideration when performing quantitative assessment of MI from the ECG. This is exemplified in Figure 4.3 which shows an example of a patient with a posterolateral transmural MI in the absence of pathological Q waves.

4.2   Q waves and QRS score versus endocardial extent of infarction (Paper II)

The pathologic basis of Q waves on the ECG after MI is still controversial. Infarct transmurality has recently been shown not to be as closely related to Q-wave MI as previously reported. Given that the first part of the QRS complex reflects depolarization of subendocardial myocardium, endocardial extent of MI is a potential determinant of pathological Q waves. The aim of this study was therefore to test the hypothesis that endocardial extent of MI is more predictive of pathological Q waves than is MI transmurality. We also sought to investigate the relationship between QRS scoring of the ECG and MI characteristics.

There was a significant difference between patients with and without Q waves
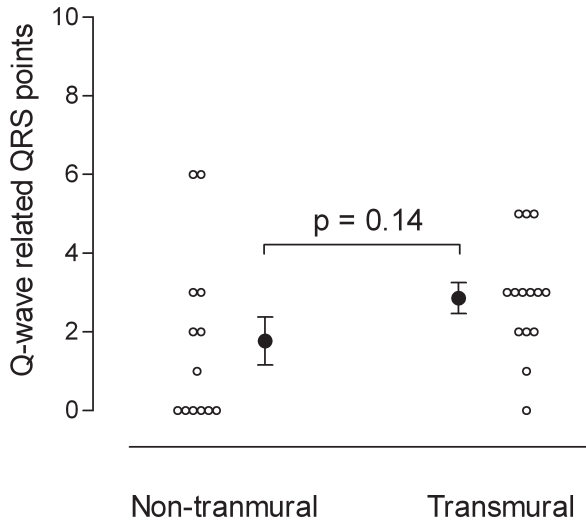
FIGURE 4.2 Comparison between non-transmural and transmural MI with regards to the number of Q-wave points awarded with QRS scoring. There was no significant difference in number of Q-wave related QRS points between the non-transmural and transmural MI groups. Solid dots indicate mean ± standard error of the mean.
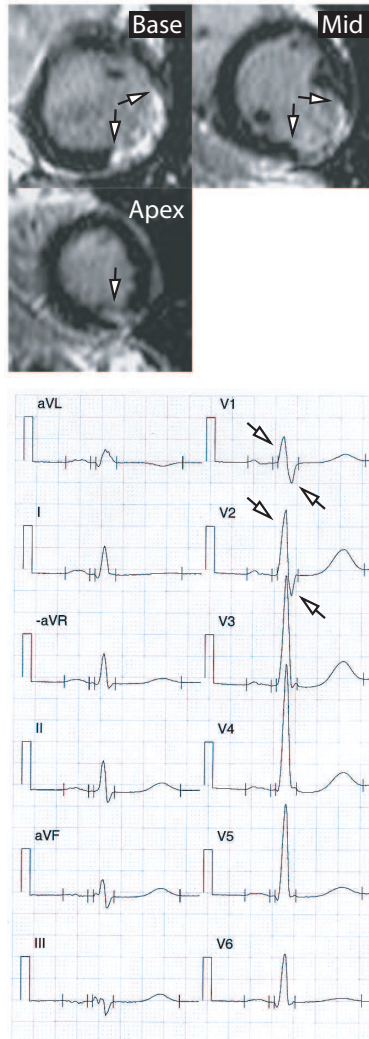
FIGURE 4.3 An example of a patient with a transmural MI in the posterolateral LV wall not associated with any pathological Q waves. The patient had prominent R-waves and small S-waves in V1 and V2 suggestive of posterolateral MI. Thus, this case illustrates the importance of considering not only Q-waves for detecting and quantifying MI by ECG. Arrows indicate either MI by DE-MRI or QRS changes generating QRS points.

with regard to MI size and endocardial extent of MI, but not with regard to mean and maximum MI transmurality (Figure 4.4).

Furthermore, endocardial extent was shown to be the only independent predictor of pathological Q waves as assessed by multivariate logistic regression analysis.

Figure 4.5 demonstrates that the endocardial extent of MI was most strongly correlated to QRS score among the MI variables examined.

Finally, QRS scoring was shown to be superior to Minnesota coding for correctly localizing the MI.

As discussed above, Q-wave appearance is dependent on the direction of the mean depolarization vector during the early parts of the QRS complex when the subendocardial portion of the myocardium is being depolarized.[151]   Thus, a subendocardial MI with a large endocardial extent has a greater likelihood of generating a Q wave in an exploring lead than has a small transmural MI with a limited endocardial extent. A small transmural MI does not necessarily influence the mean depolarization vector of the early activation enough to generate Q waves, since surrounding viable endocardial myocardium can keep the vector more or less in its original direction. These concepts are clearly demonstrated in Figure 4.6.

The superiority of the Selvester QRS scoring system for localizing MI can be explained by several features of the QRS scoring system not considered in Minnesota coding. First, R:S amplitude ratio, small Q and S waves, as well as prominent R-wave amplitude and duration in lead V1 and V2 are considered indicative of posterolateral MI. These "negative" aspects of lead V1 and V2 are not considered for Minnesota coding. Hence, lateral MIs are often missed or underestimated using Minnesota coding compared to Selvester QRS scoring.[188] This is consistent with the findings of Aguirre *et al*[187] showing that occlusion of the left circumflex artery is more common in patients with non-Q-wave MI than in patients with Q-wave MI. Second, the Selvester QRS scoring system does not only consider Q waves as sign of anterior MI in the precordial leads. Small R waves in V2–V6 as well as small R:S amplitude ratios in V4–V6 are also considered to reflect loss of myocardium due to anterior MI. This is also not considered for Minnesota coding.

4.3   Time course of infarct involution, functional recovery and ECG changes after acute infarction (Paper III)

The time course and magnitude of infarct involution, functional recovery, and normalization of infarct-related ECG changes after acute MI are not completely
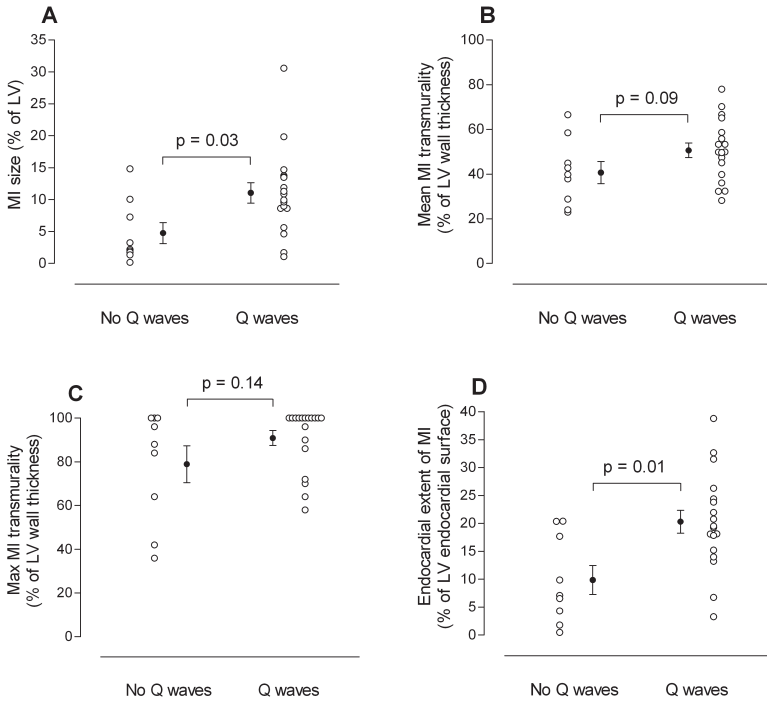
FIGURE 4.4 The relationship between the Q-wave and non-Q wave groups with regard to the different MI characteristics. Circles denote patients with infarction present on DE-MRI. Error bars indicate mean ± standard error of the mean. For MI size (**A**) and endocardial extent of MI (**D**) there was a significant difference between the two groups. Infarct transmurality (**B**,**C**), however, did not differ significantly between the two groups.
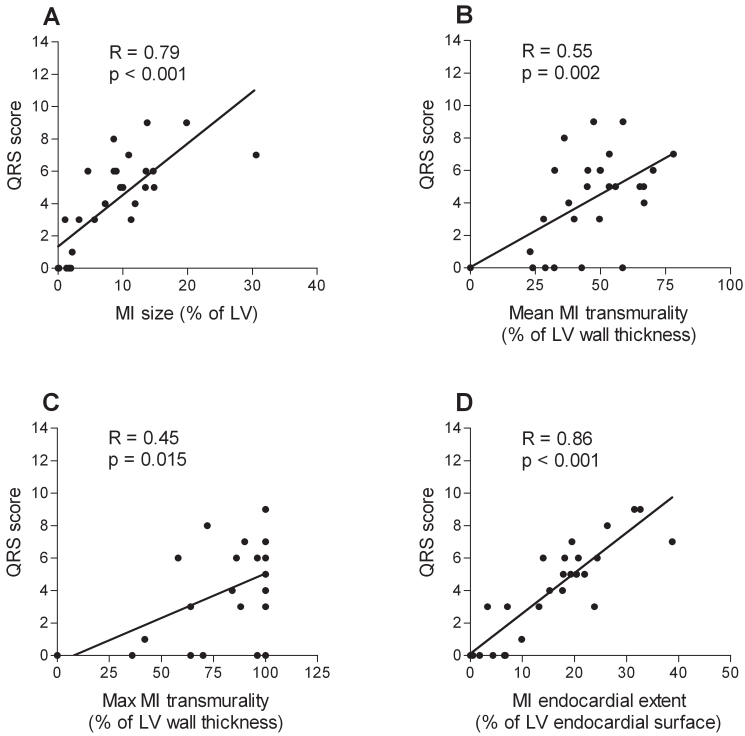
FIGURE 4.5 The relationship between global QRS score and the different MI characteristics. The global QRS score was significantly correlated to all MI characteristics examined. The strongest correlation was found between global QRS score and endocardial extent of MI.
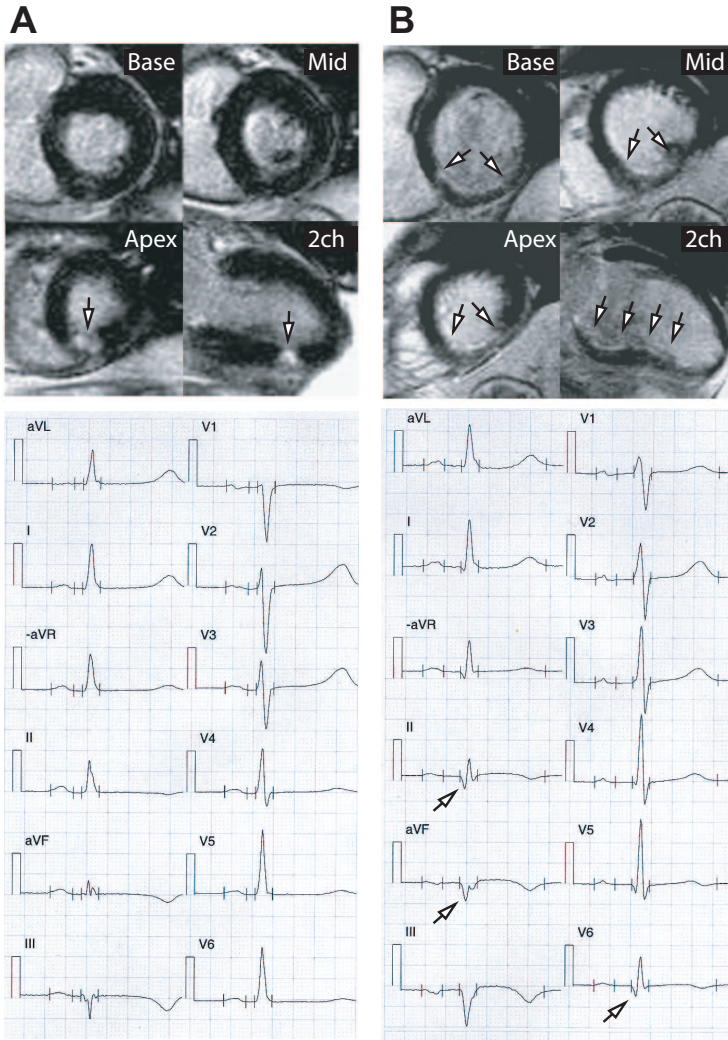
FIGURE 4.6 Two cases illustrating that endocardial extent of MI is more important than MI transmurality for the presence of pathological Q waves. **A**) A transmural inferior MI with a small endocardial extent showing no signs of pathological Q waves. **B**) A non-transmural inferior MI with a large endocardial extent associated with pathological Q waves in leads II, aVF, and V6. Arrows indicate either MI by DE-MRI or QRS changes generating QRS points.

understood in humans. Therefore, we sought to explore these processes early after MI and during one year of the infarct-healing process.

Both time course and magnitude of reduction in hyperenhanced myocardium corresponded well with normalization of the infarct-related QRS changes (Figure 4.7). The reduction was most pronounced during the first week after MI.

Figure 4.8A shows how the LV ejection fraction gradually increased over the year. Figure 4.8B demonstrates the early decrease in MI size shown in Figure 4.7 was associated with a significant increase in non-hyperenhanced myocardium during the first week after MI.

Regional wall thickening was found to decrease progressively with increasing initial transmural extent of hyperenhancement ($P_{trend}<0.0001$) (Figure 4.9). The time course of recovery in regional wall thickening differed for different transmural extents of hyperenhancement. Note that the remote myocardium improved in wall thickening during the first week. As regional MI transmurality increased the later the recovery in regional wall thickening was observed.

The pathophysiologic basis for the rapid reduction of hyperenhanced myocardium observed during the first week is somewhat controversial. Reimer and Jennings[132] have described the changing anatomic reference base of evolving MI early after acute MI. They showed that swelling of the ischemic myocardium caused by acute inflammation, edema, and hemorrhage resulted in an overestimation of MI size as assessed by histopathology.

The rapid reduction of hyperenhanced myocardium found in the present study during the first week may be explained in 2 different ways. First, a rapid reduction due to resorption of the infarcted myocardium itself, which has been proposed by Kim *et al.*[134] Second, a rapid reduction due to initial hyperenhancement of a viable periinfarction zone surrounding the irreversibly injured core of myocytes early after MI. Saeed *et al*[138] showed that MRI with the extracellular contrast agent gadopentetate dimeglumine (Gd-DTPA) overestimated the true MI size measured by triphenyltetrazolium chloride (TTC) 1 and 2 days after MI. Others have shown similar results.[135–137, 139, 189] Thus, the early reduction could partly be explained by resorption of edema and consequent loss of hyperenhancement in the viable periinfarcted zone during the first week after MI.

Enhancement of a viable periinfarction zone is likely to play a role in the reduction of hyperenhanced myocardium observed during the first week in the present study, for several reasons. First, there was a significant increase in nonhyperenhanced myocardium, which is unlikely to be explained by a significant compensatory hypertrophy during this short period. Second, almost half of the segments with >50% transmural extent of hyperenhancement at Day 1 had <50% transmural extent of hyperenhancement at Day 7. Further, the reduction of QRS score found during the first week may be explained by recruitment of viable but electrocardiographically dysfunctional myocytes in the periinfarction zone. Ursell
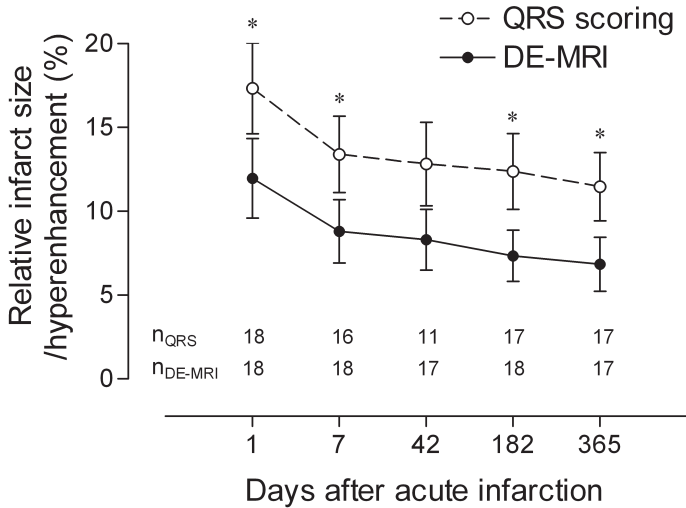
FIGURE 4.7 The relationship between normalization of infarct-related QRS changes and reduction of hyperenhanced myocardium by DE-MRI. The time course and magnitude of decrease in relative infarct size assessed by QRS scoring and reduction of hyperenhanced myocardium were similar. The infarct size by QRS scoring was, however, persistently larger than the hyperenhanced myocardium. Vertical bars indicate standard error of the mean; n_{QRS}, the number of patients that had ECG recorded at each time point; n_{DE-MRI}, the number of patients with DE-MRI at each time point; *P < 0.05 between QRS scoring and DE-MRI.
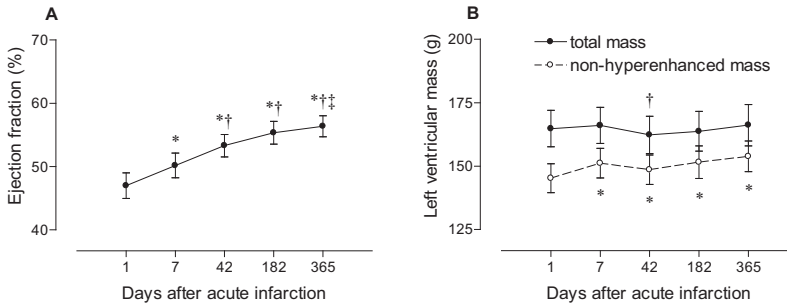
FIGURE 4.8 Changes in global left ventricular function and dimensions over time. There was a gradual increase in left ventricular ejection fraction (**A**), whereas left ventricular mass (**B**) remained relatively constant. The nonhyperenhanced myocardial mass, however, increased significantly during the first week. Vertical bars indicate standard error of the mean; *$P < 0.05$ versus Day 1; †$P < 0.05$ versus Day 7; ‡$P < 0.05$ versus Day 42.

et al[190] have shown a reversible electrophysiologic dysfunction in surviving cells from the periinfarction zone during the first 2 weeks after MI. In addition, periinfarction edema can cause conduction abnormalities,[191] which might disappear as the edema is being resorbed.

Potential mechanisms for the initial decrease in wall thickening observed in the remote and adjacent LV segments are coronary vasodilator abnormalities in the nonoccluded arteries[192] and increased systolic longitudinal wall stress due to acute alterations in LV morphology.[193]

4.4 QRS score versus infarct size and location in old anterior MI (Paper IV)

In patients with LV dysfunction associated with a clinical history of MI it is important to be able to distinguish infarcted from non-infarcted myocardium. This is important for choice of therapy since the probability for functional recovery after elective revascularization therapy depends on MI morphology.[54]

Therefore, the aim of this study was to evaluate the ability for the Selvester QRS scoring system to quantify global and regional MI size in patients with chronic ischemic heart disease and old anterior MI established by DE-MRI.

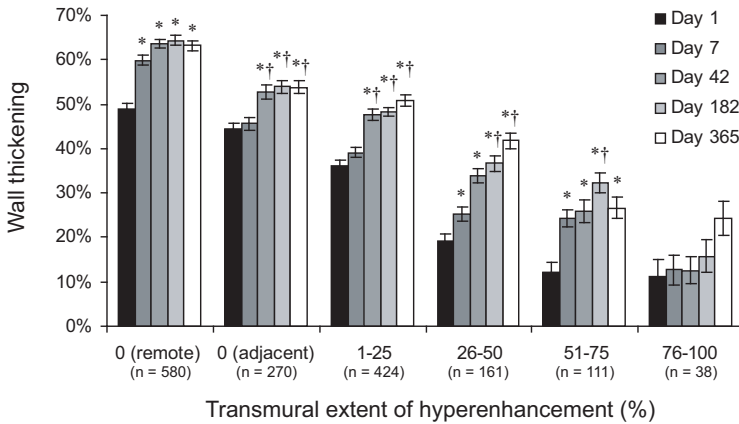There was only a moderate correlation found between QRS scoring and DE-

FIGURE 4.9 Changes in regional wall thickening over time relative to regional transmural extent of hyperenhancement at Day 1. At each time point, regional wall thickening decreased progressively with increased initial regional transmural extent of hyperenhancement. The time course for recovery of regional wall thickening also varied with regional transmural extent of hyperenhancement. Note that even the nonhyperenhanced segments showed increased wall thickening during the first week (remote) and between Day 7 and Day 42 (adjacent). Vertical bars indicate standard error of the mean; n, the number of segments in each group; *P<0.05 versus Day 1; †P<0.05 versus Day 7.

MRI with regard to relative MI size (Figure 4.10) compared to an earlier histopathology study of anterior MI.[41]

For estimation of regional MI size, the QRS scoring system performed best in the middle LV segments (Figure 4.11). The results show that the Selvester QRS scoring system significantly underestimated the extent of MI in the apical LV segments. Segments with less than 10% MI were often missed by the QRS scoring system. Thus, the area under the ROC curve increased when considering only LV segments containing more than 10% MI as positive for MI (0.80 [95% CI, 0.75–0.85] versus 0.73 [95% CI, 0.67–0.78]; >10% MI versus >0% MI).

This study differs from the previous histopathology study of anterior infarction[41] in several respects. First, none of the patients studied postmortem received reperfusion therapy, whereas most patients in this study had a reperfusion attempt at the time of the acute MI. Second, the population in the postmortem studies
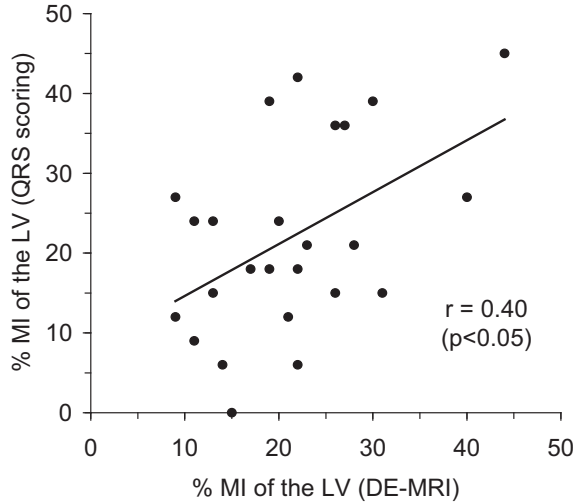
FIGURE 4.10 The relationship between MI size assessed by QRS scoring and DE-MRI in patient with severe IHD and healed MI in the anterior LV wall.

was a mixture of patients with acute and chronic MI, whereas in this study there were only patients with chronic MI. Third, the distribution of MI size in the post-mortem studies differed from the current study, with a higher number of small MIs (<10% of LV) in the former (29% vs 8%). Forth, the MI quantification procedure differed between histopathology and DE-MRI used in this study. Where the MI had caused thinning of the LV wall in the histopathology study, a reconstruction of the endocardial border was made in order to estimate the amount of myocardium that was initially subject to infarction. This type of reconstruction was not attempted in the present study. Finally, LV remodeling was most likely more severe in the present study compared to the postmortem study. In the present study, 56% (14/25) had signs of LV aneurysm caused by an infarct-related thinning of the anterior LV wall.

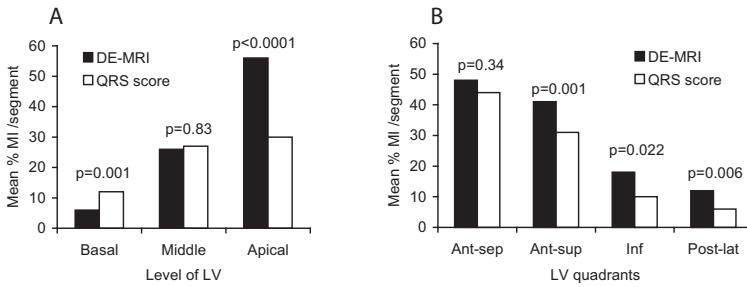The most significant difference between mean MI size per segment assessed

FIGURE 4.11 The mean % MI per segment in different parts of the LV. The bars indicate the average amount of MI by QRS scoring and DE-MRI analysis, respectively. **Left:** The 300 segments (25 patients with 12 segments each) divided into basal, mid and apical LV thirds. **Right:** The 300 segments divided into the four LV quadrants. P values indicate the difference based on paired t-test. Ant-sep indicates anteroseptal; Ant-sup, anterosuperior; DE-MRI, delayed-enhancement magnetic resonance imaging; Inf, inferior; LV, left ventricle; MI, myocardial infarction; Post-lat, posterolateral

by QRS scoring and that assessed by DE-MRI was found in the apical third of the LV (30% vs 56%). However, the correlation between the two methods for the apical segments was fairly strong (r=0.61; P<0.0001). This indicates a systematic difference in the two modalities. This could partly be explained by the minimum percentage MI of a segment given by the Selvester QRS scoring system being 13% (1/8, because 8 points in Figure 3.2, Panel B, were considered 100% MI of a segment). Thus, <13% MI per segment by DE-MRI cannot be expected to be detected with the QRS-scoring system. This can explain the improved diagnostic performance for detecting MI in segments with >10% MI compared with those with >0% MI.

Chapter 5

Conclusions

The major conclusions of the four papers are as follows:

I. QRS score is significantly related to MI size and transmurality by DE-MRI in patients with first-time reperfused MI. Presence of Q waves, however, is not indicative of transmural MI in these patients.

II. The endocardial extent of reperfused first-time MI is more predictive of pathological Q waves than is MI transmurality. Furthermore, QRS scoring is superior to Minnesota coding for correctly identifying and localizing these MIs.

III. The reduction of hyperenhanced myocardium as assessed by DE-MRI after reperfused first-time MI occurs predominantly during the first week after MI. This might reflect recovery of initially hyperenhanced but reversibly injured myocardium. There is a gradual increase in global LV function during the first year after MI. Furthermore, the time course for recovery of regional wall thickening correlates with the initial regional transmural extent of hyperenhancement, and even nonhyperenhanced myocardium shows an early increase in regional wall thickening. Finally, the time course and magnitude of reduction of hyperenhanced myocardium as assessed by DE-MRI correspond well with normalization of infarct-related ECG changes as assessed by QRS scoring.

IV. For quantifying size of old anterior MI associated with LV remodeling, the current Selvester QRS scoring system performs worse than for acute MI and for old MI not associated with LV remodeling. The diagnostic performance could potentially be improved, especially at the apex of the LV, by using DE-MRI as reference method for measuring the size and location of MI as guidance for creating new QRS criteria.

Acknowledgments

I would like to thank all the people that have helped and supported me during my time as a PhD-student and without whom this thesis would never be possible.

My supervisor, **Håkan Arheden**, for not only being a great mentor but also for always taking time to listen and share your thoughts about proffesional leadership and life in general.

My co-supervisor, **Olle Pahlm**, for your endless support and for providing such great (and fast) help with editing the manuscripts and this thesis book.

My co-supervisor, **Galen Wagner**, for providing expert advice on research in general and ECG in particular, for all the long and fruitful telephone calls, and for always believing in me.

Professor, **Björn Jonsson**, for being a leading academic star and a great representative for Clinical Physiology at the Medical Faculty, Lund University.

Ronald Selvester, for inventing and teaching me about the Selvester QRS scoring system.

Erik Hedström, for being such a great colleague and friend. Without your tremendous effort in enrolling those patients, your extraordinary computer skills, and your great sense of humor this thesis would not be possible.

Martin Ugander, for all the fun in the "4-chamber", for always taking time to listen and for keeping track of all those billions of references.

Einar Heiberg, for giving birth to and taking care of Segment, the best cardiac MRI post processing software ever made.

Marcus Carlsson, for providing your expertise in clinical cardiac MRI and for taking responsibility for all the high notes in the PhD-student quartet.

Erik Bergvall, Minna Carlsson, & Karin Markenroth, for all being great friends and colleagues.

Elin Trägårdh & John Palmer, for saving me when the statistics and mathematics kept me awake at night.

Therese Billgren, for daring to join me in my first research experiences and for being a great friend.

Richard White, Randy Setser, Sandra Halliburton, & Jane Kasper, for

taking good care of "the last viking" during his time at the Cleveland Clinic.

Kathy Shuping, Beverly Perkins, Märta Granbohm, & Karin Larsson, for all your help and patience when I was unable to keep track of all the ECGs and paperwork.

John Foster, Thomas Martin, Bjoern Groenning, & Henry Dargie, for great collaboration and for providing inspiration with scotish MALT.

Charles Maynard, Jonas Björk, & Nuray Güner, for your help when the P- and R-values were hard to get.

The staff at the Departments of **Clinical Physiology, Radiology, & Cardiology** at Lund University Hospital, and the staff at the **Department of Radiology, Section for Cardiovascular Imaging at Cleveland Clinic**, Cleveland, for supporting and helping me to complete the studies in this thesis.

My wonderful parents, **Bo-Henrik & Ann-Marie**, for your great love and support, for always caring, and for always believing in me.

My brother, **Patrik**, for sharing so much fun with me and being the best brother in world.

My sister, **Anna**, for daring to ask me for medical advices and for being the best sister in the world.

All my friends, for coping with me not being available during the last months.

Finally, my lovely wife **Tess** and my wonderful son **Axel**, for giving me the inspiration to do what I do, for all your love and support, and for letting me share my life with you.

Bibliography

[1]   Lopez A, Mathers C, Ezzati M, Jamison D, Murray C. Global and regional burden of disease and risk factors, 2001: systematic analysis of population health data. *Lancet*, 367(9524):1747–57, 2006.

[2]   Gheorghiade M, Bonow R. Chronic heart failure in the United States: a manifestation of coronary artery disease. *Circulation*, 97(3):282–9, 1998.

[3]   Van Houtven G, Honeycutt A, Gilman B, McCall N, Throneburg W. *Costs of illness for environmentally related health effects in older american*. Research Triangle Park (RTI), NC, 2005.

[4]   Nesto R, Kowalchuk G. The ischemic cascade: temporal sequence of hemodynamic, electrocardiographic and symptomatic expressions of ischemia. *Am J Cardiol*, 59(7):23C–30C, 1987.

[5]   Krachmer A. Infective endocarditis. In E Braunwald, D Zipes, P Libby, editors, *Heart disease*, pages 1723–1750. W.B. Saunders Company, Philadelphia, 6th edition, 2001.

[6]   Lip G, Gupta J, Khan M, Singh S. Recurrent myocardial infarction with angina and normal coronary arteries. *Int J Cardiol*, 51(1):65–71, 1995.

[7]   Gersh B, Bassendine M, Forman R, Walls R, Beck W. Coronary artery spasm and myocardial infarction in the absence of angiographically demonstrable obstructive coronary disease. *Mayo Clin Proc*, 56(11):700–8, 1981.

[8]   Amento E, Ehsani N, Palmer H, Libby P. Cytokines and growth factors positively and negatively regulate interstitial collagen gene expression in human vascular smooth muscle cells. *Arterioscler Thromb*, 11(5):1223–30, 1991.

[9]   Dollery C, McEwan J, Henney A. Matrix metalloproteinases and cardiovascular disease. *Circ Res*, 77(5):863–8, 1995.

[10]   Libby P. Molecular bases of the acute coronary syndromes. *Circulation*, 91(11):2844–50, 1995.

[11]   Jennings R, Murry C, Steenbergen C J, Reimer K. Development of cell injury in sustained acute ischemia. *Circulation*, 82(3 Suppl):II2–12, 1990.

[12] Jennings R, Schaper J, Hill M, Steenbergen C J, Reimer K. Effect of reperfusion late in the phase of reversible ischemic injury. Changes in cell volume, electrolytes, metabolites, and ultrastructure. *Circ Res*, 56(2):262–78, 1985.

[13] Camacho S, Figueredo V, Brandes R, Weiner M. Ca(2+)-dependent fluorescence transients and phosphate metabolism during low-flow ischemia in rat hearts. *Am J Physiol*, 265(1 Pt 2):H114–22, 1993.

[14] Meissner A, Morgan J. Contractile dysfunction and abnormal Ca2+ modulation during postischemic reperfusion in rat heart. *Am J Physiol*, 268(1 Pt 2):H100–11, 1995.

[15] Smith G, Geary G, Ruf W, Roelofs T, McNamara J. Epicardial mapping and electrocardiographic models of myocardial ischemic injury. *Circulation*, 60(4):930–8, 1979.

[16] Janse M, Cinca J, Morena H, Fiolet J, Kleber A, de Vries G, Becker A, Durrer D. The "border zone" in myocardial ischemia. An electrophysiological, metabolic, and histochemical correlation in the pig heart. *Circ Res*, 44(4):576–88, 1979.

[17] Cinca J, Figueras J, Senador G, Garcia-Moreno E, Salas A, Rius J. Transmural DC electrograms after coronary artery occlusion and latex embolization in pigs. *Am J Physiol*, 246(4 Pt 2):H475–82, 1984.

[18] Mirvis D, Goldberger A. Electrocardiography. In E Braunwald, D Zipes, P Libby, editors, *Heart Disease*, pages 82–128. W.B. Saunders Company, Philadephia, 6th edition, 2001.

[19] Sylven C. Mechanisms of pain in angina pectoris–a critical review of the adenosine hypothesis. *Cardiovasc Drugs Ther*, 7(5):745–59, 1993.

[20] Reimer K, Jennings R. The "wavefront phenomenon" of myocardial ischemic cell death. II. Transmural progression of necrosis within the framework of ischemic bed size (myocardium at risk) and collateral flow. *Lab Invest*, 40(6):633–44, 1979.

[21] Murry C, Jennings R, Reimer K. Preconditioning with ischemia: a delay of lethal cell injury in ischemic myocardium. *Circulation*, 74(5):1124–36, 1986.

[22] Birnbaum Y, Hale S, Kloner R. Progressive decrease in the ST segment elevation during ischemic preconditioning: is it related to recruitment of collateral vessels? *J Mol Cell Cardiol*, 28(7):1493–9, 1996.

[23] Marber M, Latchman D, Walker J, Yellon D. Cardiac stress protein elevation 24 hours after brief ischemia or heat stress is associated with resistance to myocardial infarction. *Circulation*, 88(3):1264–72, 1993.

[24] Kuzuya T, Hoshida S, Yamashita N, Fuji H, Oe H, Hori M, Kamada T, Tada M. Delayed effects of sublethal ischemia on the acquisition of tolerance to ischemia. *Circ Res*, 72(6):1293–9, 1993.

[25] Murry C, Richard V, Reimer K, Jennings R. Ischemic preconditioning slows energy metabolism and delays ultrastructural damage during a sustained ischemic episode. *Circ Res*, 66(4):913–31, 1990.

[26] Jennings R, Sebbag L, Schwartz L, Crago M, Reimer K. Metabolism of preconditioned myocardium: effect of loss and reinstatement of cardioprotection. *J Mol Cell Cardiol*, 33(9):1571–88, 2001.

[27] Kloner R, Yellon D. Does ischemic preconditioning occur in patients? *J Am Coll Cardiol*, 24(4):1133–42, 1994.

[28] Yellon D, Alkhulaifi A, Pugsley W. Preconditioning the human myocardium. *Lancet*, 342(8866):276–7, 1993.

[29] Schaper W, Ito W. Molecular mechanisms of coronary collateral vessel growth. *Circ Res*, 79(5):911–9, 1996.

[30] Schaper W, Gorge G, Winkler B, Schaper J. The collateral circulation of the heart. *Prog Cardiovasc Dis*, 31(1):57–77, 1988.

[31] Ganz P, Ganz W. Coronary blood flow and myocardial ischemia. In E Braunwald, D Zipes, P Libby, editors, *Heart Disease*, pages 1087–1113. W.B. Saunders Company, Philadelphia, 6th edition, 2001.

[32] Piek J, Koolen J, Hoedemaker G, David G, Visser C, Dunning A. Severity of single-vessel coronary arterial stenosis and duration of angina as determinants of recruitable collateral vessels during balloon angioplasty occlusion. *Am J Cardiol*, 67(1):13–7, 1991.

[33] Pijls N, Bech G, el Gamal M, Bonnier H, De Bruyne B, Van Gelder B, Michels H, Koolen J. Quantification of recruitable coronary collateral blood flow in conscious humans and its potential to predict future ischemic events. *J Am Coll Cardiol*, 25(7):1522–8, 1995.

[34] Sabia P, Powers E, Ragosta M, Sarembock I, Burwell L, Kaul S. An association between collateral blood flow and myocardial viability in patients with recent myocardial infarction. *N Engl J Med*, 327(26):1825–31, 1992.

[35] Charney R, Cohen M. The role of the coronary collateral circulation in limiting myocardial ischemia and infarct size. *Am Heart J*, 126(4):937–45, 1993.

[36] Alpert J, Thygesen K, Antman E, Bassand J. Myocardial infarction redefined–a consensus document of The Joint European Society of Cardiology/American College of Cardiology Committee for the redefinition of myocardial infarction. *J Am Coll Cardiol*, 36(3):959–69, 2000.

[37] Vincent G, Abildskov J, Burgess M. Mechanisms of ischemic ST-segment displacement. Evaluation by direct current recordings. *Circulation*, 56(4 Pt 1):559–66, 1977.

[38] Kleber A, Janse M, van Capelle F, Durrer D. Mechanism and time course of S-T and T-Q segment changes during acute regional myocardial ischemia in the pig heart determined by extracellular and intracellular recordings. *Circ Res*, 42(5):603–13, 1978.

[39] Dressler W, Roesler H. High T waves in the earliest stage of myocardial infarction. *Am Heart J*, 34:627–645, 1947.

[40] Goldberger A. Hyperacute T waves revisited. *Am Heart J*, 104(4 Pt 1):888–90, 1982.

[41] Ideker R, Wagner G, Ruth W, Alonso D, Bishop S, Bloor C, Fallon J, Gottlieb G, Hackel D, et al. Evaluation of a QRS scoring system for estimating myocardial infarct size. II. Correlation with quantitative anatomic findings for anterior infarcts. *Am J Cardiol*, 49(7):1604–14, 1982.

[42] Ward R, White R, Ideker R, Hindman N, Alonso D, Bishop S, Bloor C, Fallon J, Gottlieb G, et al. Evaluation of a QRS scoring system for estimating myocardial infarct size. IV. Correlation with quantitative anatomic findings for posterolateral infarcts. *Am J Cardiol*, 53(6):706–14, 1984.

[43] Roark S, Ideker R, Wagner G, Alonso D, Bishop S, Bloor C, Bramlet D, Edwards J, Fallon J, et al. Evaluation of a QRS scoring system for estimating myocardial infarct size. III. Correlation with quantitative anatomic findings for inferior infarcts. *Am J Cardiol*, 51(3):382–9, 1983.

[44] Oliva P, Hammill S, Edwards W. Electrocardiographic diagnosis of postinfarction regional pericarditis. Ancillary observations regarding the effect of reperfusion on the rapidity and amplitude of T wave inversion after acute myocardial infarction. *Circulation*, 88(3):896–904, 1993.

[45] Coll S, Betriu A, de Flores T, Roig E, Sanz G, Mont L, Magrina J, Serra A, Navarro Lopez F. Significance of Q-wave regression after transmural acute myocardial infarction. *Am J Cardiol*, 61(10):739–42, 1988.

[46] Pappas M. Disappearance of pathological Q waves after cardiac infarction. *Br Heart J*, 20(1):123–8, 1958.

[47] Kalbfleisch J, Shadaksharappa K, Conrad L, Sarkar N. Disappearance of the Q-deflection following myocardial infarction. *Am Heart J*, 76(2):193–8, 1968.

[48] Albert D, Califf R, LeCocq D, McKinnis R, Ideker R, Wagner G. Comparative rates of resolution of QRS changes after operative and nonoperative acute myocardial infarcts. *Am J Cardiol*, 51(3):378–81, 1983.

[49] Lyck F, Holmvang L, Grande P, Madsen J, Wagner G, Clemmensen P. Effects of revascularization after first acute myocardial infarction on the evolution of QRS complex changes (the DANAMI trial). DANish Trial in Acute Myocardial Infarction. *Am J Cardiol*, 83(4):488–92, 1999.

[50] Holman E, van Jonbergen H, van Dijkman P, van der Laarse A, de Roos A, van der Wall E. Comparison of magnetic resonance imaging studies with enzymatic indexes of myocardial necrosis for quantification of myocardial infarct size. *Am J Cardiol*, 71(12):1036–40, 1993.

[51] Haase J, Bayar R, Hackenbroch M, Storger H, Hofmann M, Schwarz C, Reinemer H, Schwarz F, Ruef J, Sommer T. Relationship between size of myocardial infarctions assessed by delayed contrast-enhanced MRI after primary PCI, biochemical markers, and time to intervention. *J Interv Cardiol*, 17(6):367–73, 2004.

[52] Ingkanisorn W, Rhoads K, Aletras A, Kellman P, Arai A. Gadolinium delayed enhancement cardiovascular magnetic resonance correlates with clinical measures of myocardial infarction. *J Am Coll Cardiol*, 43(12):2253–9, 2004.

[53] Choi K, Kim R, Gubernikoff G, Vargas J, Parker M, Judd R. Transmural extent of acute myocardial infarction predicts long-term improvement in contractile function. *Circulation*, 104(10):1101–7, 2001.

[54] Kim R, Wu E, Rafael A, Chen E, Parker M, Simonetti O, Klocke F, Bonow R, Judd R. The use of contrast-enhanced magnetic resonance imaging to identify reversible myocardial dysfunction. *N Engl J Med*, 343(20):1445–53, 2000.

[55] Persson E, Palmer J, Pettersson J, Warren S, Borges-Neto S, Wagner G, Pahlm O. Quantification of myocardial hypoperfusion with 99m Tc-sestamibi in patients undergoing prolonged coronary artery balloon occlusion. *Nucl Med Commun*, 23(3):219–28, 2002.

[56] Pfeffer M, Braunwald E. Ventricular remodeling after myocardial infarction. Experimental observations and clinical implications. *Circulation*, 81(4):1161–72, 1990.

[57] Braunwald E, Kloner R. The stunned myocardium: prolonged, postischemic ventricular dysfunction. *Circulation*, 66(6):1146–9, 1982.

[58] Kloner R, Ellis S, Lange R, Braunwald E. Studies of experimental coronary artery reperfusion. Effects on infarct size, myocardial function, biochemistry, ultrastructure and microvascular damage. *Circulation*, 68(2 Pt 2):I8–15, 1983.

[59] Rahimtoola S. The hibernating myocardium. *Am Heart J*, 117(1):211–21, 1989.

[60] Nienaber C, Brunken R, Sherman C, Yeatman L, Gambhir S, Krivokapich J, Demer L, Ratib O, Child J, et al. Metabolic and functional recovery of ischemic human myocardium after coronary angioplasty. *J Am Coll Cardiol*, 18(4):966–78, 1991.

[61] Takeishi Y, Tono-oka I, Kubota I, Ikeda K, Masakane I, Chiba J, Abe S, Tsuiki K, Komatani A, et al. Functional recovery of hibernating myocardium after coronary bypass surgery: does it coincide with improvement in perfusion? *Am Heart J*, 122(3 Pt 1):665–70, 1991.

[62] Ugander M, Cain P, Johnsson P, Palmer J, Arheden H. Influence of the presence of chronic non-transmural myocardial infarction on the time course of perfusion and functional recovery after revascularization. *Submitted for publication*.

[63] Weisman H, Bush D, Mannisi J, Weisfeldt M, Healy B. Cellular mechanisms of myocardial infarct expansion. *Circulation*, 78(1):186–201, 1988.

[64] Colucci W, Braunwald E. Pathophysiology of the heart. In E Braunwald, D Zipes, P Libby, editors, *Heart Disease*, pages 503–533. W.B. Saunders Company, Philadephia, 6th edition, 2001.

[65] Steg P, Dabbous O, Feldman L, Cohen-Solal A, Aumont M, Lopez-Sendon J, Budaj A, Goldberg R, Klein W, Anderson FA J. Determinants and prognostic impact of heart failure complicating acute coronary syndromes: observations from the Global Registry of Acute Coronary Events (GRACE). *Circulation*, 109(4):494–9, 2004.

[66] Kashani A, Giugliano R, Antman E, Morrow D, Gibson C, Murphy S, Braunwald E. Severity of heart failure, treatments, and outcomes after fibrinolysis in patients with ST-elevation myocardial infarction. *Eur Heart J*, 25(19):1702–10, 2004.

[67] Hasdai D, Topol E, Kilaru R, Battler A, Harrington R, Vahanian A, Ohman E, Granger C, Van de Werf F, et al. Frequency, patient characteristics, and outcomes of mild-to-moderate heart failure complicating ST-segment elevation acute myocardial infarction: lessons from 4 international fibrinolytic therapy trials. *Am Heart J*, 145(1):73–9, 2003.

[68] Cowie M, Wood D, Coats A, Thompson S, Poole-Wilson P, Suresh V, Sutton G. Incidence and aetiology of heart failure; a population-based study. *Eur Heart J*, 20(6):421–8, 1999.

[69] Spencer F, Meyer T, Gore J, Goldberg R. Heterogeneity in the management and outcomes of patients with acute myocardial infarction complicated by heart failure: the National Registry of Myocardial Infarction. *Circulation*, 105(22):2605–10, 2002.

[70] Ali A, Rybicki B, Alam M, Wulbrecht N, Richer-Cornish K, Khaja F, Sabbah H, Goldstein S. Clinical predictors of heart failure in patients with first acute myocardial infarction. *Am Heart J*, 138(6 Pt 1):1133–9, 1999.

[71] Moller J, Brendorp B, Ottesen M, Kober L, Egstrup K, Poulsen S, Torp-Pedersen C. Congestive heart failure with preserved left ventricular systolic function after acute myocardial infarction: clinical and prognostic implications. *Eur J Heart Fail*, 5(6):811–9, 2003.

[72] Anavekar N, McMurray J, Velazquez E, Solomon S, Kober L, Rouleau J, White H, Nordlander R, Maggioni A, et al. Relation between renal dysfunction and cardiovascular outcomes after myocardial infarction. *N Engl J Med*, 351(13):1285–95, 2004.

[73] Bayes de Luna A, Coumel P, Leclercq J. Ambulatory sudden cardiac death: mechanisms of production of fatal arrhythmia on the basis of data from 157 cases. *Am Heart J*, 117(1):151–9, 1989.

[74] Campbell R, Murray A, Julian D. Ventricular arrhythmias in first 12 hours of acute myocardial infarction. Natural history study. *Br Heart J*, 46(4):351–7, 1981.

[75] Bello D, Fieno D, Kim R, Pereles F, Passman R, Song G, Kadish A, Goldberger J. Infarct morphology identifies patients with substrate for sustained ventricular tachycardia. *J Am Coll Cardiol*, 45(7):1104–8, 2005.

[76] Denniss A, Richards D, Waywood J, Yung T, Kam C, Ross D, Uther J. Electrophysiological and anatomic differences between canine hearts with inducible ventricular tachycardia and fibrillation associated with chronic myocardial infarction. *Circ Res*, 64(1):155–66, 1989.

[77] Schoen F. The heart. In F Cotran, V Kumar, T Collins, editors, *Pathologic basis of disease*, pages 543–599. W.B. Saunders Company, Philadelphia, 6th edition, 1999.

[78] Aoyagi T, Pouleur H, Van Eyll C, Rousseau M, Mirsky I. Wall motion asynchrony is a major determinant of impaired left ventricular filling in patients with healed myocardial infarction. *Am J Cardiol*, 72(3):268–72, 1993.

[79] Brutsaert D. Nonuniformity: a physiologic modulator of contraction and relaxation of the normal heart. *J Am Coll Cardiol*, 9(2):341–8, 1987.

[80] GUSTO. An international randomized trial comparing four thrombolytic strategies for acute myocardial infarction. The GUSTO investigators. *N Engl J Med*, 329(10):673–82, 1993.

[81] Chesebro J, Knatterud G, Roberts R, Borer J, Cohen L, Dalen J, Dodge H, Francis C, Hillis D, et al. Thrombolysis in Myocardial Infarction (TIMI) Trial, Phase I: A comparison between intravenous tissue plasminogen activator and intravenous streptokinase. Clinical findings through hospital discharge. *Circulation*, 76(1):142–54, 1987.

[82] Grip L. Reperfusionsbehandling med trombolys och PCI. In L Wallentin, editor, *Akut kranskärlssjukdom*, pages 80–90. Liber AB, Stockholm, 3rd edition, 2005.

[83] Montalescot G, Barragan P, Wittenberg O, Ecollan P, Elhadad S, Villain P, Boulenc J, Morice M, Maillard L, et al. Platelet glycoprotein IIb/IIIa inhibition with coronary stenting for acute myocardial infarction. *N Engl J Med*, 344(25):1895–903, 2001.

[84] Keeley E, Boura J, Grines C. Primary angioplasty versus intravenous thrombolytic therapy for acute myocardial infarction: a quantitative review of 23 randomised trials. *Lancet*, 361(9351):13–20, 2003.

[85] Packer M, Bristow M, Cohn J, Colucci W, Fowler M, Gilbert E, Shusterman N. The effect of carvedilol on morbidity and mortality in patients with chronic heart failure. U.S. Carvedilol Heart Failure Study Group. *N Engl J Med*, 334(21):1349–55, 1996.

[86] Pitt B, Segal R, Martinez F, Meurers G, Cowley A, Thomas I, Deedwania P, Ney D, Snavely D, Chang P. Randomised trial of losartan versus captopril in patients over 65 with heart failure (Evaluation of Losartan in the Elderly Study, ELITE). *Lancet*, 349(9054):747–52, 1997.

[87] Braunwald E. Expanding indications for beta-blockers in heart failure. *N Engl J Med*, 344(22):1711–2, 2001.

[88] Metaanalysis. Collaborative meta-analysis of randomised trials of antiplatelet therapy for prevention of death, myocardial infarction, and stroke in high risk patients. *Bmj*, 324(7329):71–86, 2002.

[89] Patrono C, Bachmann F, Baigent C, Bode C, De Caterina R, Charbonnier B, Fitzgerald D, Hirsh J, Husted S, et al. Expert consensus document on the use of antiplatelet agents. The task force on the use of antiplatelet agents in patients with atherosclerotic cardiovascular disease of the European society of cardiology. *Eur Heart J*, 25(2):166–81, 2004.

[90] Yusuf S, Zhao F, Mehta S, Chrolavicius S, Tognoni G, Fox K. Effects of clopidogrel in addition to aspirin in patients with acute coronary syndromes without ST-segment elevation. *N Engl J Med*, 345(7):494–502, 2001.

[91] Mehta S, Yusuf S, Peters R, Bertrand M, Lewis B, Natarajan M, Malmberg K, Rupprecht H, Zhao F, et al. Effects of pretreatment with clopidogrel and aspirin followed by long-term therapy in patients undergoing percutaneous coronary intervention: the PCI-CURE study. *Lancet*, 358(9281):527–33, 2001.

[92] Adgey A. An overview of the results of clinical trials with glycoprotein IIb/IIIa inhibitors. *Am Heart J*, 135(4):S43–55, 1998.

[93] Schreuder J, Castiglioni A, Maisano F, Steendijk P, Donelli A, Baan J, Alfieri O. Acute decrease of left ventricular mechanical dyssynchrony and improvement of contractile state and energy efficiency after left ventricular restoration. *J Thorac Cardiovasc Surg*, 129(1):138–45, 2005.

[94] AVID. A comparison of antiarrhythmic-drug therapy with implantable defibrillators in patients resuscitated from near-fatal ventricular arrhythmias. The Antiarrhythmics versus Implantable Defibrillators (AVID) Investigators. *N Engl J Med*, 337(22):1576–83, 1997.

[95] Bergfeldt L. CABG and ICD for all patients with hemodynamically significant ventricular arrhythmia and significant coronary artery disease? Do we know enough to decide–or to design a randomized trial? *Pacing Clin Electrophysiol*, 22(8):1129–31, 1999.

[96] Hauer R, Aliot E, Block M, Capucci A, Luderitz B, Santini M, Vardas P. Indications for implantable cardioverter defibrillator (ICD) therapy. Study Group on Guidelines on ICDs of the Working Group on Arrhythmias and the Working Group on Cardiac Pacing of the European Society of Cardiology. *Eur Heart J*, 22(13):1074–81, 2001.

[97] Rackley C. Value of ventriculography in cardiac function and diagnosis. *Cardiovasc Clin*, 6(3):283–96, 1975.

[98] Jansson K, Fransson S. Mortality related to coronary angiography. *Clin Radiol*, 51(12):858–60, 1996.

[99] Raff G, Gallagher M, O'Neill W, Goldstein J. Diagnostic accuracy of noninvasive coronary angiography using 64-slice spiral computed tomography. *J Am Coll Cardiol*, 46(3):552–7, 2005.

[100] Leschka S, Alkadhi H, Plass A, Desbiolles L, Grunenfelder J, Marincek B, Wildermuth S. Accuracy of MSCT coronary angiography with 64-slice technology: first experience. *Eur Heart J*, 26(15):1482–7, 2005.

[101] Shaw L, Raggi P, Schisterman E, Berman D, Callister T. Prognostic value of cardiac risk factors and coronary artery calcium screening for all-cause mortality. *Radiology*, 228(3):826–33, 2003.

[102] Schlosser T, Pagonidis K, Herborn C, Hunold P, Waltering K, Lauenstein T, Barkhausen J. Assessment of left ventricular parameters using 16-MDCT and new software for endocardial and epicardial border delineation. *AJR Am J Roentgenol*, 184(3):765–73, 2005.

[103] Yamamuro M, Tadamura E, Kubo S, Toyoda H, Nishina T, Ohba M, Hosokawa R, Kimura T, Tamaki N, et al. Cardiac functional analysis with multi-detector row CT and segmental reconstruction algorithm: comparison with echocardiography, SPECT, and MR imaging. *Radiology*, 234(2):381–90, 2005.

[104] Mahnken A, Koos R, Katoh M, Spuentrup E, Busch P, Wildberger J, Kuhl H, Gunther R. Sixteen-slice spiral CT versus MR imaging for the assessment of left ventricular function in acute myocardial infarction. *Eur Radiol*, 15(4):714–20, 2005.

[105] Mahnken A, Koos R, Katoh M, Wildberger J, Spuentrup E, Buecker A, Gunther R, Kuhl H. Assessment of myocardial viability in reperfused acute myocardial infarction using 16-slice computed tomography in comparison to magnetic resonance imaging. *J Am Coll Cardiol*, 45(12):2042–7, 2005.

[106] Andrieu N, Easton D, Chang-Claude J, Rookus M, Brohet R, Cardis E, Antoniou A, Wagner T, Simard J, et al. Effect of Chest X-Rays on the Risk of Breast Cancer Among BRCA1/2 Mutation Carriers in the International BRCA1/2 Carrier Cohort Study. *J Clin Oncol*, 2006.

[107] Gutierrez-Chico J, Zamorano J, Perez de Isla L, Orejas M, Almeria C, Rodrigo J, Ferreiros J, Serra V, Macaya C. Comparison of left ventricular volumes and ejection fractions measured by three-dimensional echocardiography versus by two-dimensional echocardiography and cardiac magnetic resonance in patients with various cardiomyopathies. *Am J Cardiol*, 95(6):809–13, 2005.

[108] Hatle L, Sutherland G. Regional myocardial function–a new approach. *Eur Heart J*, 21(16):1337–57, 2000.

[109] Dilsizian V, Perrone-Filardi P, Arrighi J, Bacharach S, Quyyumi A, Freedman N, Bonow R. Concordance and discordance between stress-redistribution-reinjection and rest-redistribution thallium imaging for assessing viable myocardium. Comparison with metabolic activity by positron emission tomography. *Circulation*, 88(3):941–52, 1993.

[110] Germano G, Berman D. *Clinical gated cardiac SPECT*. Futura Publishing Company, Armonk, New York, 1999.

[111] Bax J, Lamb H, Dibbets P, Pelikan H, Boersma E, Viergever E, Germano G, Vliegen H, de Roos A, et al. Comparison of gated single-photon emission computed tomography with magnetic resonance imaging for evaluation of left ventricular function in ischemic cardiomyopathy. *Am J Cardiol*, 86(12):1299–305, 2000.

[112] Tadamura E, Kudoh T, Motooka M, Inubushi M, Okada T, Kubo S, Hattori N, Matsuda T, Koshiji T, et al. Use of technetium-99m sestamibi ECG-gated single-photon emission tomography for the evaluation of left ventricular function following coronary artery bypass graft: comparison with three-dimensional magnetic resonance imaging. *Eur J Nucl Med*, 26(7):705–12, 1999.

[113] Tadamura E, Kudoh T, Motooka M, Inubushi M, Shirakawa S, Hattori N, Okada T, Matsuda T, Koshiji T, et al. Assessment of regional and global left ventricular function by reinjection T1-201 and rest Tc-99m sestamibi ECG-gated SPECT: comparison with three-dimensional magnetic resonance imaging. *J Am Coll Cardiol*, 33(4):991–7, 1999.

[114] Schelbert H, Wisenberg G, Phelps M, Gould K, Henze E, Hoffman E, Gomes A, Kuhl D. Noninvasive assessment of coronary stenoses by myocardial imaging during pharmacologic coronary vasodilation. VI. Detection of coronary artery disease in human beings with intravenous N-13 ammonia and positron computed tomography. *Am J Cardiol*, 49(5):1197–207, 1982.

[115] Slart R, Bax J, de Jong R, de Boer J, Lamb H, Mook P, Willemsen A, Vaalburg W, van Veldhuisen D, Jager P. Comparison of gated PET with MRI for evaluation of left ventricular function in patients with coronary artery disease. *J Nucl Med*, 45(2):176–82, 2004.

[116] Schaefer W, Lipke C, Nowak B, Kaiser H, Buecker A, Krombach G, Buell U, Kuhl H. Validation of an evaluation routine for left ventricular volumes, ejection fraction and wall motion from gated cardiac FDG PET: a comparison with cardiac magnetic resonance imaging. *Eur J Nucl Med Mol Imaging*, 30(4):545–53, 2003.

[117] Bax J. FDG imaging should be considered the preferred technique for accurate assessment of myocardial viability: for. *Eur J Nucl Med Mol Imaging*, 32(7):829–31, 2005.

[118] Tsao J, Boesiger P, Pruessmann K. k-t BLAST and k-t SENSE: dynamic MRI with high frame rate exploiting spatiotemporal correlations. *Magn Reson Med*, 50(5):1031–42, 2003.

[119] Larson A, Kellman P, Arai A, Hirsch G, McVeigh E, Li D, Simonetti O. Preliminary investigation of respiratory self-gating for free-breathing segmented cine MRI. *Magn Reson Med*, 53(1):159–68, 2005.

[120] Kellman P, Larson A, Hsu L, Chung Y, Simonetti O, McVeigh E, Arai A. Motion-corrected free-breathing delayed enhancement imaging of myocardial infarction. *Magn Reson Med*, 53(1):194–200, 2005.

[121] Engblom H, Hedstrom E, Palmer J, Wagner G, Arheden H. Determination of the left ventricular long-axis orientation from a single short-axis MR image: relation to BMI and age. *Clin Physiol Funct Imaging*, 24(5):310–5, 2004.

[122] Arheden H, Holmqvist C, Thilen U, Hanseus K, Bjorkhem G, Pahlm O, Laurin S, Stahlberg F. Left-to-right cardiac shunts: comparison of measurements obtained with MR velocity mapping and with radionuclide angiography. *Radiology*, 211(2):453–8, 1999.

[123] Bergvall E, Cain P, Arheden H, Sparr G. A fast and highly automated approach to myocardial motion analysis using phase contrast magnetic resonance imaging. *J Magn Reson Imaging*, 23(5):652–61, 2006.

[124] Kwong R, Chan A, Brown K, Chan C, Reynolds H, Tsang S, Davis R. Impact of unrecognized myocardial scar detected by cardiac magnetic resonance imaging on event-free survival in patients presenting with signs or symptoms of coronary artery disease. *Circulation*, 113(23):2733–43, 2006.

[125] Weinmann H, Brasch R, Press W, Wesbey G. Characteristics of gadolinium-DTPA complex: a potential NMR contrast agent. *AJR Am J Roentgenol*, 142(3):619–24, 1984.

[126] Kroll H, Korman S, Siegel E, Hart H, Rosoff B, Spencer H, Laszlo D. Excretion of yttrium and lanthanum chelates of cyclohexane 1,2-trans diamine tetraacetic acid and diethylenetriamine pentaacetic acid in man. *Nature*, 180(4592):919–20, 1957.

[127] Klein C, Nekolla S, Balbach T, Schnackenburg B, Nagel E, Fleck E, Schwaiger M. The influence of myocardial blood flow and volume of distribution on late Gd-DTPA kinetics in ischemic heart failure. *J Magn Reson Imaging*, 20(4):588–93, 2004.

[128] Tong C, Prato F, Wisenberg G, Lee T, Carroll E, Sandler D, Wills J, Drost D. Measurement of the extraction efficiency and distribution volume for Gd-DTPA in normal and diseased canine myocardium. *Magn Reson Med*, 30(3):337–46, 1993.

[129] Saeed M, Wendland M, Masui T, Higgins C. Reperfused myocardial infarctions on T1- and susceptibility-enhanced MRI: evidence for loss of compartmentalization of contrast media. *Magn Reson Med*, 31(1):31–9, 1994.

[130] Arheden H, Saeed M, Higgins C, Gao D, Bremerich J, Wyttenbach R, Dae M, Wendland M. Measurement of the distribution volume of gadopentetate dimeglumine at echo-planar MR imaging to quantify myocardial infarction: comparison with 99mTc-DTPA autoradiography in rats. *Radiology*, 211(3):698–708, 1999.

[131] Flacke S, Fischer S, Lorenz C. Measurement of the gadopentetate dimeglumine partition coefficient in human myocardium in vivo: normal distribution and elevation in acute and chronic infarction. *Radiology*, 218(3):703–10, 2001.

[132] Reimer K, Jennings R. The changing anatomic reference base of evolving myocardial infarction. Underestimation of myocardial collateral blood flow and overestimation of experimental anatomic infarct size due to tissue edema, hemorrhage and acute inflammation. *Circulation*, 60(4):866–76, 1979.

[133] Hedstrom E, Arheden H, Eriksson R, Johansson L, Ahlstrom H, Bjerner T. Importance of perfusion in myocardial viability studies using delayed contrast-enhanced magnetic resonance imaging. *J Magn Reson Imaging*, 24(1):77–83, 2006.

[134] Kim R, Fieno D, Parrish T, Harris K, Chen E, Simonetti O, Bundy J, Finn J, Klocke F, Judd R. Relationship of MRI delayed contrast enhancement to irreversible injury, infarct age, and contractile function. *Circulation*, 100(19):1992–2002, 1999.

[135] Schaefer S, Malloy C, Katz J, Parkey R, Buja L, Willerson J, Peshock R. Gadolinium-DTPA-enhanced nuclear magnetic resonance imaging of reperfused myocardium: identification of the myocardial bed at risk. *J Am Coll Cardiol*, 12(4):1064–72, 1988.

[136] Nishimura T, Yamada Y, Hayashi M, Kozuka T, Nakatani T, Noda H, Takano H. Determination of infarct size of acute myocardial infarction in dogs by magnetic resonance imaging and gadolinium-DTPA: comparison with indium-111 antimyosin imaging. *Am J Physiol Imaging*, 4(3):83–8, 1989.

[137] Saeed M, Bremerich J, Wendland M, Wyttenbach R, Weinmann H, Higgins C. Reperfused myocardial infarction as seen with use of necrosis-specific versus standard extracellular MR contrast media in rats. *Radiology*, 213(1):247–57, 1999.

[138] Saeed M, Lund G, Wendland M, Bremerich J, Weinmann H, Higgins C. Magnetic resonance characterization of the peri-infarction zone of reperfused myocardial infarction with necrosis-specific and extracellular nonspecific contrast media. *Circulation*, 103(6):871–6, 2001.

[139] Arheden H, Saeed M, Higgins C, Gao D, Ursell P, Bremerich J, Wyttenbach R, Dae M, Wendland M. Reperfused rat myocardium subjected to various durations of ischemia: estimation of the distribution volume of contrast material with echo-planar MR imaging. *Radiology*, 215(2):520–8, 2000.

[140] Abildgaard P. Tentamina electrica in animalibus. *Inst Soc Med Havn*, 2:157–161, 1775.

[141] Galvani L. De viribus electritatis in muto musculari commentarius. 1791.

[142] Burdon Sanderson J. Experimental results relating to the rhythmical and excitatory motions of the ventricle of the frog. *Proc R Soc Lond*, 27:410–414, 1878.

[143] Waller A. On the electromotive changes connected with the beat of the mammalian heart, and of the human heart in particular. *Philos Trans R Soc*, 180:169–94, 1889.

[144] Einthoven W. Ueber die From des menschlichen Electrocardiogramms. *Arch f d Ges Physiol*, 60:101–123, 1895.

[145] Einthoven W. Le telecardiogramme. *Arch Int de Physiol*, 4:132–164 (translated into English in Am Heart J 1957;53:602–615), 1906.

[146] Pardee H. An electrocardiographic sign of coronary artery obstruction. *Arch Int Med*, 26:244–257, 1920.

[147] Wilson F, Johnston F, MacLeod A, Barker P. Electrocardiograms that represent the potential variations of a single electrode. *Am Heart J*, 9:447–458, 1934.

[148] Barnes A, Pardee H, White P, Wilson F, Wolferth C. Standardization of precordial leads. *Am Heart J*, 15:235–239, 1938.

[149] Goldberger E. A simple, indifferent, electrocardiographic electrode of zero potential and a technique of obtaining augmented, unipolar, extremity leads. *Am Heart J*, 23:483–492, 1942.

[150] Holter N, Generelli J. Remote recording of physiologic data by radio. *Rocky Mountain Med J*, pages 747–751, 1949.

[151] Durrer D, van Dam R, Freud G, Janse M, Meijler F, Arzbaecher R. Total excitation of the isolated human heart. *Circulation*, 41(6):899–912, 1970.

[152] Kubota I, Yamaki M, Shibata T, Ikeno E, Hosoya Y, Tomoike H. Role of ATP-sensitive K+ channel on ECG ST segment elevation during a bout of myocardial ischemia. A study on epicardial mapping in dogs. *Circulation*, 88(4 Pt 1):1845–51, 1993.

[153] Boden W, Kleiger R, Gibson R, Schwartz D, Schechtman K, Capone R, Roberts R. Electrocardiographic evolution of posterior acute myocardial infarction: importance of early precordial ST-segment depression. *Am J Cardiol*, 59(8):782–7, 1987.

[154] Mandel W, Burgess M, Neville J J, Abildskov J. Analysis of T-wave abnormalities associated with myocardial infarction using a theoretic model. *Circulation*, 38(1):178–88, 1968.

[155] Prinzmetal M, Shaw CM J, Maxwell M, Flamm E, Goldman A, Kimura N, Rakita L, Borduas J, Rothman S, Kennamer R. Studies on the mechanism of ventricular activity. VI. The depolarization complex in pure subendocardial infarction; role of the subendocardial region in the normal electrocardiogram. *Am J Med*, 16(4):469–89, 1954.

[156] Phibbs B. "Transmural" versus "subendocardial" myocardial infarction: an electrocardiographic myth. *J Am Coll Cardiol*, 1(2 Pt 1):561–4, 1983.

[157] Pipberger H, Lopez E. "Silent" subendocardial infarcts: fact or fiction? *Am Heart J*, 100(5):597–9, 1980.

[158] Spodick D. Q-wave infarction versus S-T infarction. Nonspecificity of electrocardiographic criteria for differentiating transmural and nontransmural lesions. *Am J Cardiol*, 51(5):913–5, 1983.

[159] Moon J, De Arenaza D, Elkington A, Taneja A, John A, Wang D, Janardhanan R, Senior R, Lahiri A, et al. The pathologic basis of Q-wave and non-Q-wave myocardial infarction: a cardiovascular magnetic resonance study. *J Am Coll Cardiol*, 44(3):554–60, 2004.

[160] Kaandorp T, Bax J, Lamb H, Viergever E, Boersma E, Poldermans D, van der Wall E, de Roos A. Which parameters on magnetic resonance imaging determine Q waves on the electrocardiogram? *Am J Cardiol*, 95(8):925–9, 2005.

[161] Engblom H, Hedstrom E, Heiberg E, Wagner G, Pahlm O, Arheden H. Size and transmural extent of first-time reperfused myocardial infarction assessed by cardiac magnetic resonance can be estimated by 12-lead electrocardiogram. *Am Heart J*, 150(5):920, 2005.

[162] Wu E, Judd R, Vargas J, Klocke F, Bonow R, Kim R. Visualisation of presence, location, and transmural extent of healed Q-wave and non-Q-wave myocardial infarction. *Lancet*, 357(9249):21–8, 2001.

[163] Selvester R, Wagner G, Ideker R. Myocardial infarction. In P Macfarlane, T Lawrie, editors, *Comprehensive electrocardiology: Theory and practice in health and disease*, volume 1, pages 566–629. Pergamon press, New York, 1st edition, 1989.

[164] Wagner G, Freye C, Palmeri S, Roark S, Stack N, Ideker R, Harrell FE J, Selvester R. Evaluation of a QRS scoring system for estimating myocardial infarct size. I. Specificity and observer agreement. *Circulation*, 65(2):342–7, 1982.

[165] Jones M, Anderson K, Wilson P, Kannel W, Wagner N, Wagner G. Prognostic use of a QRS scoring system after hospital discharge for initial acute myocardial infarction in the Framingham cohort. *Am J Cardiol*, 66(5):546–50, 1990.

[166] Bounous EP J, Califf R, Harrell FE J, Hinohara T, Mark D, Ideker R, Selvester R, Wagner G. Prognostic value of the simplified Selvester QRS score in patients with coronary artery disease. *J Am Coll Cardiol*, 11(1):35–41, 1988.

[167] Jones M, Ramo B, Raff G, Hinohara T, Wagner G. Evaluation of methods of measurement and estimation of left ventricular function after acute myocardial infarction. *Am J Cardiol*, 56(12):753–6, 1985.

[168] Palmeri S, Harrison D, Cobb F, Morris K, Harrell F, Ideker R, Selvester R, Wagner G. A QRS scoring system for assessing left ventricular function after myocardial infarction. *N Engl J Med*, 306(1):4–9, 1982.

[169] Anderson W, Wagner N, Lee K, White R, Yuschak J, Behar V, Selvester R, Ideker R, Wagner G. Evaluation of a QRS scoring system for estimating myocardial infarct size. VI: Identification of screening criteria for non-acute myocardial infarcts. *Am J Cardiol*, 61(10):729–33, 1988.

[170] Engblom H, Wagner G, Setser R, Selvester R, Billgren T, Kasper J, Maynard C, Pahlm O, Arheden H, White R. Quantitative clinical assessment of chronic anterior myocardial infarction with delayed enhancement magnetic resonance imaging and QRS scoring. *Am Heart J*, 146(2):359–66, 2003.

[171] Horacek B, Warren J, Albano A, Palmeri M, Rembert J, Greenfield JC J, Wagner G. Development of an automated Selvester Scoring System for estimating the size of myocardial infarction from the electrocardiogram. *J Electrocardiol*, 39(2):162–8, 2006.

[172] Howe C, Freye C, Wagner N, Leggett S, Behar J, Jones M, Hinohara T, Wagner G. Evaluation of a QRS scoring system for estimating myocardial infarct size. VII: Specificity in a control group with right ventricular hypertrophy due to mitral stenosis. *Am J Cardiol*, 62(4):322–4, 1988.

[173] Freye C, Wagner N, Howe C, Stack N, Ideker R, Selvester R, Wagner G. Evaluation of a QRS scoring system for estimating myocardial infarct size. VIII. Specificity in a control group with left ventricular hypertrophy and proposal of a new scoring system for use with this confounding factor. *J Electrocardiol*, 25(1):19–23, 1992.

[174] Haisty WK J, Pahlm O, Wagner N, Pope J, Wagner G. Performance of the automated complete Selvester QRS scoring system in normal subjects and patients with single and multiple myocardial infarctions. *J Am Coll Cardiol*, 19(2):341–6, 1992.

[175] Sevilla D, Wagner N, Pegues R, Peck S, Mikat E, Ideker R, Hutchins G, Reimer K, Hackel D, et al. Correlation of the complete version of the Selvester QRS scoring system with quantitative anatomic findings for multiple left ventricular myocardial infarcts. *Am J Cardiol*, 69(5):465–9, 1992.

[176] Macfarlane P. Normal limits. In P Macfarlane, T Lawrie, editors, *Comprehensive electrocardiology: Theory and practice in health and disease*, volume 3, page 1441. Pergamon press, New York, 1st edition, 1989.

[177] Pahlm O, Haisty WK J, Wagner N, Pope J, Wagner G. Specificity and sensitivity of QRS criteria for diagnosis of single and multiple myocardial infarcts. *Am J Cardiol*, 68(13):1300–4, 1991.

[178] Selvester R, Wagner G, Ideker R, Gates K, Starr S, Ahmed J, Crump R. ECG myocardial infarct size: a gender-, age-, race-insensitive 12-segment multiple regression model. I: Retrospective learning set of 100 pathoanatomic infarcts and 229 normal control subjects. *J Electrocardiol*, 27 Suppl:31–41, 1994.

[179] Pennell D. Ventricular volume and mass by CMR. *J Cardiovasc Magn Reson*, 4(4):507–13, 2002.

[180] Simonetti O, Kim R, Fieno D, Hillenbrand H, Wu E, Bundy J, Finn J, Judd R. An improved MR imaging technique for the visualization of myocardial infarction. *Radiology*, 218(1):215–23, 2001.

[181] Heiberg E, Engblom H, Engvall J, Hedstrom E, Ugander M, Arheden H. Semi-automatic quantification of myocardial infarction from delayed contrast enhanced magnetic resonance imaging. *Scand Cardiovasc J*, 39(5):267–75, 2005.

[182] Pope J, Wagner N, Dubow D, Edmonds J, Wagner G, Haisty WK J. Development and validation of an automated method of the Selvester QRS scoring system for myocardial infarct size. *Am J Cardiol*, 61(10):734–8, 1988.

[183] Pahlm O, Haisty WK J, Wagner N, Selvester R, Pope J, Wagner G. Performance of the automated complete Selvester QRS scoring system. *J Electrocardiol*, 23 Suppl:28, 1990.

[184] Macfarlane P, Lawrie T. Coding schemes. In P Macfarlane, T Lawrie, editors, *Comprehensive electrocardiology: Theory and practice in health and disease*, volume 3, pages 1567–1582. Pergamon press, New York, 1st edition, 1989.

[185] Stone P, Raabe D, Jaffe A, Gustafson N, Muller J, Turi Z, Rutherford J, Poole W, Passamani E, et al. Prognostic significance of location and type of myocardial infarction: independent adverse outcome associated with anterior location. *J Am Coll Cardiol*, 11(3):453–63, 1988.

[186] Benhorin J, Moss A, Oakes D. Prognostic significance of nonfatal myocardial re-infarction. Multicenter Diltiazem Postinfarction Trial Research Group. *J Am Coll Cardiol*, 15(2):253–8, 1990.

[187] Aguirre F, Younis L, Chaitman B, Ross A, McMahon R, Kern M, Berger P, Sopko G, Rogers W, et al. Early and 1-year clinical outcome of patients' evolving non-Q-wave versus Q-wave myocardial infarction after thrombolysis. Results from The TIMI II Study. *Circulation*, 91(10):2541–8, 1995.

[188] Pahlm U, Chaitman B, Rautaharju P, Selvester R, Wagner G. Comparison of the various electrocardiographic scoring codes for estimating anatomically documented sizes of single and multiple infarcts of the left ventricle. *Am J Cardiol*, 81(7):809–15, 1998.

[189] Choi S, Jiang C, Lim K, Kim S, Lim C, Gong G, Lim T. Application of breath-hold T2-weighted, first-pass perfusion and gadolinium-enhanced T1-weighted MR imaging for assessment of myocardial viability in a pig model. *J Magn Reson Imaging*, 11(5):476–80, 2000.

[190] Ursell P, Gardner P, Albala A, Fenoglio JJ J, Wit A. Structural and electrophysiological changes in the epicardial border zone of canine myocardial infarcts during infarct healing. *Circ Res*, 56(3):436–51, 1985.

[191] Gloviczki P, Solti F, Szlavy L, Jellinek H. Ultrastructural and electrophysiologic changes of experimental acute cardiac lymphostasis. *Lymphology*, 16(3):185–92, 1983.

[192] Uren N, Crake T, Lefroy D, de Silva R, Davies G, Maseri A. Reduced coronary vasodilator function in infarcted and normal myocardium after myocardial infarction. *N Engl J Med*, 331(4):222–7, 1994.

74

[193] Bogaert J, Bosmans H, Maes A, Suetens P, Marchal G, Rademakers F. Remote myocardial dysfunction after acute anterior myocardial infarction: impact of left ventricular shape on regional function: a magnetic resonance myocardial tagging study. *J Am Coll Cardiol*, 35(6):1525–34, 2000.

Papers I–IV